POLITECNICO
MILANO 1863

SCUOLA DI INGEGNERIA INDUSTRIALE
E DELL'INFORMAZIONE

A Multibody Approach for Spacecraft Docking

Tesi di Laurea Magistrale in
Space Engineering - Ingegneria Spaziale

Author: **Tommaso Aresi**

Student ID: 971092
Advisor: Prof. Pierangelo Masarati
Academic Year: 2021-22

Abstract

Rendez-Vous Docking or Berthing (RVD/B) technology and techniques are used to re-supply orbital platforms and stations, switch crews in orbital stations, repair spacecraft in orbit, retrieve and capture spacecraft to bring them back to Earth and re-join orbiting vehicles from the ground. Docking is the act of two spacecraft joining and sealing to one another with a Guidance Navigation and Control (GNC) system active until the first touch. This thesis models a docking system using multibody dynamics, for its integration into algorithms for optimization of guidance and navigation, or attitude and dynamics determination and control.

The system is described in the International Docking System Standard and aims to simulate multibody docking mechanics, considering more accurate off-nominal situations. The thesis deal with the system modelization from a different point of view with respect to via Finite Element Method (FEM) are suitable, FEM is suitable for detailed mechanical analysis, but balancing the computational efficiency and accuracy required in an integrated design calls for a different approach. This work tries to provide a design tool, taking into account the docking simulation from its early stages. On the opposite, an approach expressing and coding the Equations of Motion directly should constrain the model to a specific problem, not easily enabling a straight way to improve hierarchically the simulation.

The aim of this thesis work is to define a proper simulation environment to model both the docking dynamics and control logic in the most embedded way between different fields such as GNC design, Attitude Determination and Control System (ADCS) design, Multibody System Dynamics design and Structures and Mechanisms design, in this way the docking problem can be fully addressed.

Keywords: Spacecraft Docking, Multibody Dynamics, Embedded Design, Relative Navigation

Abstract in lingua italiana

Il Rendez-Vous Docking o Berthing (RVD/B) con le sue tecnologie e tecniche è il modo tramite il quale si riesce a rifornire le stazioni orbitali, scambiarne gli equipaggi, riparare le navicelle spaziali e i satelliti, recuperare e catturare i satelliti per riportarli sulla Terra o ricongiungersi con i veicoli in orbita, partendo dal suolo. Il docking viene definito come l'atto di due veicoli spaziali che attraccano e si pressurizzano tramite un sistema di Guidance Navigation and Control (GNC) attivo fino al primo tocco. Questa tesi cerca modellare il sistema di attracco dal punto di vista della dinamica multibody, per la sua integrazione in algoritmi come l'ottimizzazione della guida, navigazione e controllo e la determinazione dell'assetto e dinamica del veicolo.

Il sistema presentato è descritto nell'International Docking System Standard e mira a simulare la meccanica del docking, provando a definire situazioni non-nominali più accurate. La modellazione e la simulazione del docking può essere effettuata tramite il metodo degli elementi finiti, adatti per l'analisi meccanica dettagliata, ma non a bilanciare l'efficienza computazionale e l'accuratezza richieste in un design integrato. Questo lavoro fornisce un primo strumento di progettazione, tenendo conto della simulazione del docking, fin dalle sue prime fasi. Al contrario, una modellazione che scriva direttamente le equazioni del moto non permetterebbe di mantenere semplice l'integrazione di sviluppi futuri, così che l'idea di avere un carattere generale dello studio venga meno.

L'obiettivo di questa tesi è di definire un ambiente di simulazione adeguato al fine di modellare l'attracco e la logica di controllo nel modo più integrato possibile tra diversi campi dell'ingegneria spaziale, come il design della GNC o il design dell'Attitude Determination and Control System (ADCS) oppure la progettazione della dinamica dei sistemi Multibody o delle Strutture e Mecchanismi, tutto ciò per affrontare un design del docking nella maniera più completa.

Parole chiave: Spacecraft Docking, Multibody Dynamics, Embedded Design, Relative Navigation

Contents

Executive Summary

ABSTRACT

This thesis models a docking system using multibody dynamics, for its integration into algorithms like optimization of the guidance and navigation or the attitude determination and control. The system is described in the International Docking System Standard and aims to simulate docking mechanics, trying to consider more accurate off-nominal situations. The finite element method is suitable for detailed mechanical analysis of the docking process, but balancing the computational efficiency and accuracy required in an integrated design calls for a different approach. This work provides a design tool, taking into account the docking simulation from the early stages.

Keywords: Spacecraft Docking.

INTRODUCTION

Rendez-Vous Docking or Berthing (RVD/B) technology and techniques are used to re-supply orbital platforms and stations, switch crews in orbital stations, repair spacecraft in orbit, retrieve and capture spacecraft to bring them back to Earth, and re-join orbiting vehicles from the ground. Docking is the act of two spacecraft joining and sealing to one another with a Guidance Navigation and Control (GNC) system active until the first touch. [1]

It is important to define a proper simulation environment in order to model both the docking dynamics and control logic in the most embedded way between different fields such as GNC design, Attitude Determination and Control System (ADCS) design, Multibody System Dynamics design or Structures and Mechanisms design.

MULTIBODY MODEL

This thesis refers to the IDSS Interface Docking Document (IDSS IDD) [2] guidelines for materials and mass properties of docking system and approaching spacecraft. The system is modeled in MBDyn (`https://mbdyn.org/`) [3, 4] for its versatility and light computation burden, defining multibody entities such as elements (bodies and joints) and nodes.

The system is divided into three body elements: the International Space Station-Hosting Vehicle (HV), the approaching spacecraft-Visiting Vehicle (VV), and the Visiting Vehicle Soft Capture System (SCS). Each element has its own set of properties and parameters that describe its behavior within the system, such as mass, inertia, and geometry.

Structural nodes have *6* degrees of freedom, representing position and orientation in the 3D space, and thus describe the kinematics of rigid-body motion in space. The three bodies are dynamic nodes with inertia that provide linear and angular momenta degrees of freedom. Dummy structural nodes, rigidly connected to the dynamic ones, are used to visualize the kinematics of arbitrary points during the simulation. The modeling was made hierarchically.

NDSB1	Guide Petal	SCS Ring	HCS Plane
Material	$7075-T7351$	"	2219-Al
density, g/cc	2.81	"	2.84
Young's Modulus, GPa	72	"	73.1
Poisson Ratio,	0.33	"	"
Shear Modulus, GPa	26.9	"	27.0
Yield Strength, MPa	434	"	350

Table 1: NDSB1 material properties

Vehicles	m, kg	I_{xx}, kg·m^2	I_{yy}, kg·m^2	I_{zz}, kg·m^2
IDSS	5000	$34 \cdot 10^3$	$18 \cdot 10^3$	$18 \cdot 10^3$
SCS	40	12.67	6.42	6.42
HCS	300	579.4	450	452

Table 2: Visiting vehicles inertia properties

In MBDyn a joint is an element that connects, in a prescribed way, different rigid bodies within a multibody system. There are several types of joints available, each with its own set of parameters that define its behavior. Joints may have internal degrees of freedom when they introduce kinematic constraints in form of algebraic relationships between the coordinates of the nodes they connect. By defining the properties of each joint element,

	X	Y	Z
IDSS	2.3	0	0
SCS	0.015	0	0
HCS	0.165	0.356	0.0045

Table 3: X, Y, Z coordinates of the capture system mating plane center, m

and combining them together with the other elements, the system can be fully described. Joint elements used in this complex mechanical system are total joints (selective constrain components of relative displacement and rotation between parts), rods, and deformable displacement joints (establishing relative configuration-dependent forces between parts), allowing for precise control over the motion of connected bodies. The model presents *15* joint elements:

- *6* rods between Hard Capture System (HCS) and SCS, modeling the linear actuator system (LAS);
- *1* driven total joint between SCS and ISS; it clamps the nodes when the mating systems are close enough so that latches strikers impose a constrain along the motion axis;
- *1* driven total joint between HCS and ISS; it clamps the nodes when the mating systems are close enough so that the HCS active and passive hooks constrain the capture system;
- *1* driven total joint imposes the velocity of the HCS node, simulating the Guidance, Navigation, and Control (GNC) system;
- *1* total joint between HCS ans SCS, this imposes a slider between the HCS and SCS, it is then deleted, it is used for preliminary settings to reduce modeling uncertainties;
- *1* total joint between HCS ISS nodes, this imposes a slider between the HCS and SCS, it is then deleted, it is used for preliminary settings to reduce modeling uncertainties;
- *1* total joint on ISS, it clamps the ISS and can be deleted, in a first approximation ISS is not free to move;

The actuation elements are implemented using the prescribed strain, ε_p, of rod elements, namely

$$F = F(\varepsilon - \varepsilon_p, \dot{\varepsilon}) \tag{1}$$

which is formulated according to the control logic of the docking system. Their rather

sophisticated constitutive law is implemented in a dedicated user-defined module, a specific docking module with the state machine and control logic, following NASA guidelines. The 6 rods are arranged in a Stewart platform fashion, with 3 couples of hinges on the SCS and 3 couples of mirrored hinges on the HCS.

Joint elements are also used to model the contacts. The contact between latch and striker is provided by driving a rod joint element. The contact between the petals is modeled using deformable displacement joints, with instances of the continuous contact module (`cont-contact`) in the direction normal to the surface to model finite contact areas. Contact at an angle with respect to the tangent plane can cause the outgoing velocity and angle to be significant enough to allow the object to fall freely.

The regions in the mating systems where the contact can occur are the edges of the petals and the latches and strikers spots. Given the dimensions of the edge limiting the contact area $a = 0.3$ m and $b = 0.011$ m, given the orientations of each area, the contacts are geometrically well defined. The dimensions on the edges enforce the minimum number of contact points: *30* for each edge for a total of *180* contact points and relative contact joint.

The contacts module requires the characterization of its parameters to model the contact force. The formulation proposed in [5, 6] with restitution coefficient $e_{\text{res}} = 0.6$, stiffness $k_{\text{el}} = 2 \cdot 10^3$, exponent $n = 1.5$ is used.

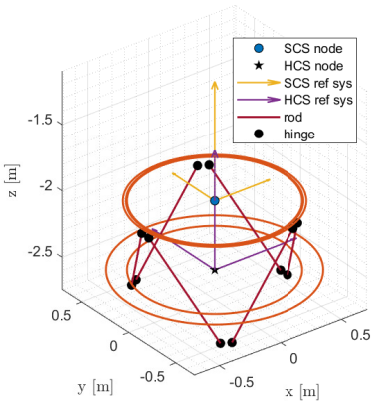

Figure 1: Geometry of the Docking System

STATES AND CONTROL

This thesis simulates the NASA Docking System Block 1 (NDSB1) [7] since it is the standardized docking system developed by NASA for use in various space missions. It uses

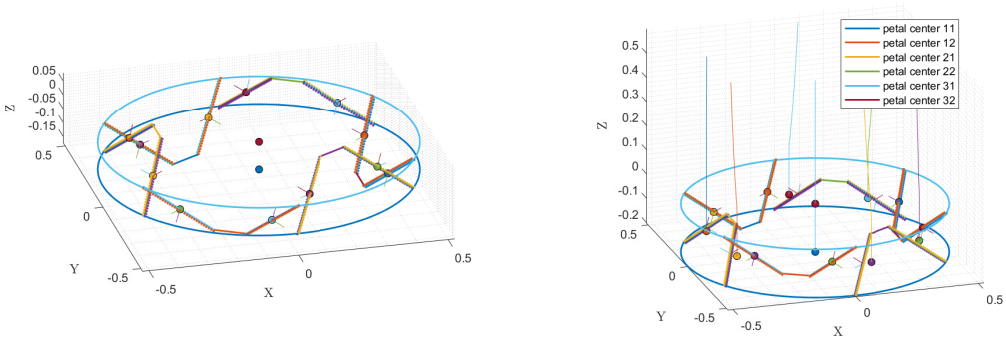

(a) Contact nodes nominal displacement (b) Contact nodes off-nominal interaction

Figure 2: Contact nodes displacements

a "state machine" to represent the system's behavior as a series of states and transitions between those states. The modes or states defined by the state machine are described in NASA documentation and are managed by the Linear Actuator System (LAS). The conditions to trigger the state change are stated below, with each transition requiring to be in the previous state to have a sequential ordering.

The aforementioned defined modes are 7: *INITIAL*, *EXTRACTION*, *LUNGE*, *ATTENUATION*, *ALIGNMENT*, *RETRACTION*, *STRUCTURAL MATING*.

- The condition to pass from INITIAL to EXTRACTION mode is that the spacecraft overcome a threshold distance, in this simulation, the triggering distance is $d^{\text{sc}}_{\text{extraction}} < 3$ m.
- Any contact between the docking system is required to transition from extraction to lunge mode. This implies accounting for any of the contact joints aforementioned, $\sum_i F_{\text{cont}_i} > 0$.
- The condition to pass from LUNGE to ATTENUATION mode: each latch is engaged to its striker within a certain tolerance, such that $||\mathbf{x}_{\text{latch}_i} - \mathbf{x}_{\text{striker}_i}|| < \text{tol}$, where $\text{tol} = 0.0005$ m.
- The condition to pass from ATTENUATION to ALIGNMENT mode is that the spacecraft's kinetic energy is below a tolerance, $E^{\text{SC}}_{\text{kin}} < \text{tol}$, where $\text{tol} = 0.001$.
- The condition to pass from ALIGNMENT to RETRACTION mode is that each actuator length l_{LAS_i} is at the prescribed elongation l_{target} within a strict tolerance, $|l_{\text{LAS}_i} - l_{\text{target}}| < \text{tol}$, where $\text{tol} = 0.01$ m.
- The condition to pass from RETRACTION to STRUCTURAL MATING mode is

that the elongation of LAS is small enough to allow structural hooks engagement, such that $|l_{\mathrm{LAS}_i} - l^{\mathrm{SM}}_{\mathrm{target}}| < \mathrm{tol}$ with $l^{\mathrm{SM}}_{\mathrm{target}} = 0.2$ m and $\mathrm{tol} = 0.001$ m.

A new module was written in C++ for MBDyn to manage all states and control laws, as well as define a new driver to drive joints to turn them on and off. The thesis proposes a saturated Proportional-Derivative (PD) control on each actuator's displacement and velocity, independent for each actuator, to limit the total force put on the mating ring and structure behind it. This behavior continues until the state machine's trigger for the next phase. An important aspect is that straightforward formulation of NASA guidelines [7–9] like the one written below can lead to discontinuities in numerical computation.

$$\begin{cases} F = k_p(u - u_{\mathrm{target}}) + k_d(\dot{u} - \dot{u}_{\mathrm{target}}) & \text{if } |F| < F_{\max} \\ F = F_{\max} & \text{if } |F| \geq F_{\max} \end{cases} \tag{2}$$

To address this, scenarios were investigated to find a solution.

1. making use of some linking polynomials all the way up to a finite continuity of class n;
2. to optimize a parametric sigmoid function with the constraints of zeros and slopes, with the goal of minimizing the approximation error;
3. to locate an effective mollifier by making use of the results of Urysohn's lemma.

The first method includes at least $2N(n+1)$ parameters for each of the N discontinuity points (surfaces for higher dimensions) and each of the n continuity classes.

The second strategy's manipulation of the sigmoids did not have enough degrees of freedom to simultaneously recover the slope in the zeros locus and the "time" to reach steady conditions. The new sigmoidal proposed by Liying Cao and other, [10] sigmoidal patterns like generalized logistic or Gompertz's function were covered, but they suffer from the aforementioned and coupling parameters problems. It is useful to stress here the conditions and constraints that such a parametric smooth function shall accomplish:

1. At infinite its behavior shall not differ from the constant behavior of the original piecewise-linear function: $|f(\mathbf{x} \to \infty, \mathbf{k})| = F_{\max}$.
2. Its value at the discontinuity point shall be tunable: $f(\mathbf{x} = \hat{\mathbf{x}}, \mathbf{k}) = \lambda F_{\max}$. Otherwise, an optimality constraint shall be imposed such as minimizing the squared mismatches.
3. Its value should be the same as the value of the original piecewise-linear function in

a certain part of the domain (in zero's loci in this case): $f(\mathbf{x} = \mathbf{x}_0, \mathbf{k}) = \tilde{f} = 0$.

4. In the same loci its slope shall be the same as the original piecewise-linear function: $f(\mathbf{x} = \mathbf{x}_0, \mathbf{k})_{|\mathbf{x}} = \boldsymbol{\alpha}$.
5. The cylindrical symmetry condition with respect to the zero's loci line: $f(-(\mathbf{x} - \mathbf{x}_0), \mathbf{k}) = -f((\mathbf{x} - \mathbf{x}_0), \mathbf{k})$.

The third strategy ought to be effective; however, it should make it possible to avoid direct convolution and integration in the software, and it ought to provide directly tunable flexibility.

The application of a linear description, in accordance with Victor M. Jimenez-Fernandez [11] and O. Chua's works [12–14], offers an n-dimensional infinite continuity class function with a tunable error that can be managed with just one parameter more than the bare minimum set for piece-wise functions. Ochua canonical representation followed these steps to provide its compact formulation:

- Given $f = f(\mathbf{x})$ with $\mathbf{x} \in \mathbf{R}^n$.
- Defined the ith linear partition of $\mathbf{R}^n$ such as $\boldsymbol{\alpha}_i^\top \mathbf{x} = \beta_i$.
- Given the non-degenerate partition of $\mathbf{R}^n$ in p hyperplanes.
- Defined the pseudo-unbounded, the essentially-unbounded regions $\mathbf{R}_{j\infty}$ and their amount number k.
- Defined two adjacent regions associated with the ith hyperplane where their sign-sequence vectors differ only at the ith position as $\mathbf{R_{i+}}$ and $\mathbf{R_{i-}}$.

$$
\begin{aligned}
\mathbf{b} &= \frac{1}{k} \sum_{j=1}^{k} \nabla f(\mathbf{x}) \Big|_{\mathbf{R_{j\infty}}} \qquad a = f(\mathbf{0}) - \sum_{i=1}^{p} c_i |\boldsymbol{\beta}_i| \\
c_i &= \frac{1}{2} \frac{\boldsymbol{\alpha}_i^\top (\nabla f(\mathbf{x})|_{\mathbf{R}_{i+}} - \nabla f(\mathbf{x})|_{\mathbf{R_{i-}}})}{\boldsymbol{\alpha}^\top \boldsymbol{\alpha}} \\
f(\mathbf{x}) &= a + \mathbf{b}^\top \mathbf{x} + \sum_{i=1}^{p} c_i |\boldsymbol{\alpha}_i^\top \mathbf{x} - \beta_i|
\end{aligned}
\tag{3}
$$

Victor M. Jimenez-Fernandez's work was used to create a smoothed representation of the standard piecewise-linear control model. The result is a differentiable formulation preserving the parameters of the original model, allowing for control of the smoothness grade and approximation accuracy at specific break-point locations.

When the curvature is too high, this notation has some overflow problems, which can be

solved by using a multi-objective optimization approach. This approach tries to minimize both the approximation error and the governing parameter by utilizing a weighted utopia method. Analytically, it can be useful to understand the relation between the max error e_{max} and λ, even if a least square method is used.

$$\begin{aligned} A &= a - \sum_{i=1}^{p} c_i\beta_i; \qquad B = b + \sum_{i=1}^{p} c_i; \\ C_i &= \frac{2c_i}{\lambda}; \qquad \hat{B} = B + \sum_{i=1}^{p} c_i\boldsymbol{\alpha}_i; \\ f(\mathbf{x}) &= A + \hat{B}^\top\mathbf{x} + \sum_{i=1}^{p} C_i \log\left(1 + \mathrm{e}^{\lambda(\boldsymbol{\alpha}^\top\mathbf{x}-\beta_i)}\right); \end{aligned} \tag{4}$$

$$e_{max_i} = \frac{2c_i\log(2)}{\lambda_i} = \log(2)C_i; \tag{5}$$

- Given two breaking lines so $p = 2$:

$$\begin{aligned} h_1: \quad & k_1(u-u_0) + k_2(\dot{u}-\dot{u}_0) = -F_{max}; && \boldsymbol{\alpha}_1 = [k_1, k_2]^\top; \\ h_2: \quad & k_1(u-u_0) + k_2(\dot{u}-\dot{u}_0) = F_{max}; && \boldsymbol{\alpha}_2 = [k_1, k_2]^\top; \\ & \beta_1 = -F_{max} + k_1u_0 + k_2\dot{u}_0; \\ & \beta_2 = F_{max} + k_1u_0 + k_2\dot{u}_0; \end{aligned} \tag{6}$$

- Given two essentially unbounded regions, $k = 2$
- Defining:

$$\mathbf{R}_{1\infty} = \mathbf{R}_{1-}; \qquad \mathbf{R}_{2\infty} = \mathbf{R}_{2+}; \qquad \mathbf{R}_{\mathbf{1}+} = \mathbf{R}_{\mathbf{2}-}; \tag{7}$$

- Computing:

$$f_{|\mathbf{x}|_{\mathbf{R}_{1-}}} = \mathbf{0}; \qquad f_{|\mathbf{x}|_{\mathbf{R}_{1+}}} = f_{|\mathbf{x}|_{\mathbf{R}_{2-}}} = [k_1, k_2]^\top; \qquad f_{|\mathbf{x}|_{\mathbf{R}_{\mathbf{2}+}}} = \mathbf{0}; \tag{8}$$

The canonical representation, with the minimum parameter set, is defined as:

$$\begin{aligned} &\mathbf{b} = \mathbf{0}; \qquad c_1 = 1/2; \qquad c_2 = -1/2; \\ &a = f(\mathbf{0}) - \frac{1}{2}|-F_{max} + k_1u_0 + k_2\dot{u}_0| + \frac{1}{2}|F_{max} + k_1u_0 + k_2\dot{u}_0|; \end{aligned} \tag{9}$$

$$f(\mathbf{x}) = \Big\{ f(\mathbf{0}) - \frac{1}{2}(|k_1 u_0 + k_2 \dot{u}_0 - F_{\max}| - |k_1 u_0 + k_2 \dot{u}_0 + F_{\max}| + \\ - |k_1(u - u_0) + k_2(\dot{u} - \dot{u}_0) + F_{\max}| + |k_1(u - u_0) + k_2(\dot{u} - \dot{u}_0) - F_{\max}|) \Big\}; \tag{10}$$

It is now provided the actual implemented non-linear control law:

$$\begin{aligned} & A = f(\mathbf{0}) + F_{\max} - \frac{1}{2}| - F_{\max} + k_1 u_0 + k_2 \dot{u}_0| + \frac{1}{2}|F_{\max} + k_1 u_0 + k_2 \dot{u}_0|; \\ & \hat{\mathbf{B}} = \mathbf{0}; \qquad C_1 = 1/\lambda; \qquad C_2 = 1/\lambda; \end{aligned} \tag{11}$$

$$f(\mathbf{x}) = \Big\{ f(\mathbf{0}) + F_{\max} - \frac{1}{2}\left(|k_1 u_0 + k_2 \dot{u}_0 - F_{\max}| - |k_1 u_0 + k_2 \dot{u}_0 + F_{\max}| + \right. \tag{12}$$

$$- \frac{2}{\lambda} \log\left(1 + \mathrm{e}^{-\lambda(k_1(u-u_0)+k_2(\dot{u}-\dot{u}_0)+F_{\max})}\right) + \tag{13}$$

$$\left. + \frac{2}{\lambda} \log\left(1 + \mathrm{e}^{-\lambda(k_1(u-u_0)+k_2(\dot{u}-\dot{u}_0)-F_{\max})}\right) \right) \Big\};$$

For a two-dimensional control law, the number of parameters of this formulation is the minimum one, just seven: $f(\mathbf{x})$, $F_{\max}$, u_0, $\dot{u}_0$, $\lambda_1 = \lambda_2 = \lambda$, k_1 and k_2. This function is tunable and respects all constraints. It adds one parameter, λ, to enforce infinite order smoothness while selecting a linking polynomial for continuity implies ten more parameters in one dimension. With this control law tuned for each docking mode, it implies 70 more than the already required parameters for the piecewise-linear formulation with respect to the seven with the presented smoothing process.

Another result is the formulation of a new one-dimensional sigmoidal function that can overcome the issues of Liying Cao and colleagues, the tanh expression, and the generalized logistic function. It provides the smallest possible group of parameters and decoupled parameters, making the initial guess more guessable and the process of optimizing the data fit more simple.

$$x_1 = \frac{F_1}{m} + x_0; \qquad x_2 = \frac{F_2}{m} + x_0; \tag{14}$$

$$f(x) = F(0) + \frac{m}{2}\left(-|x_1| + |x_2| - x_1 + x_2 + \frac{2}{\alpha_1}\log\left(1 + \mathrm{e}^{-\alpha_1(x-x_1)}\right) - \frac{2}{\alpha_2}\log\left(1 + \mathrm{e}^{-\alpha_2(x-x_2)}\right)\right)$$

Where there are just six parameters, F_1 for the lower asymptote, F_2 for the upper asymptote, m for the slope in x_0, x_0 the zero passing point and α_1 and α_2 complying for the curvature in the slope change points. If symmetry is imposed and required just four

remain, $F(0)$, F_{lim}, m, α.

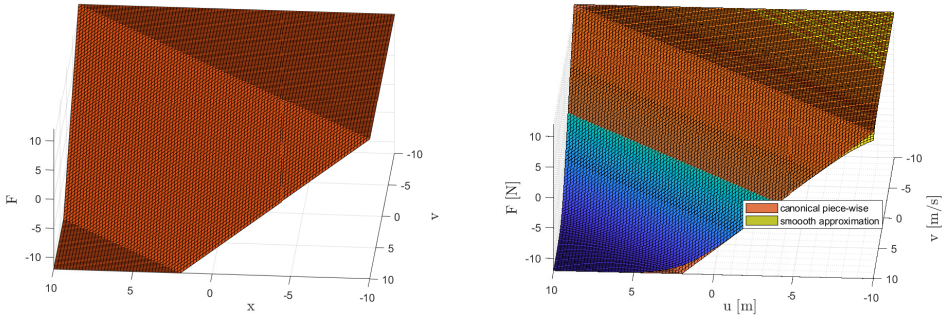

(a) Control law directly from NASA (b) Control law after smoothing process

Figure 3: Dummy control laws for understanding

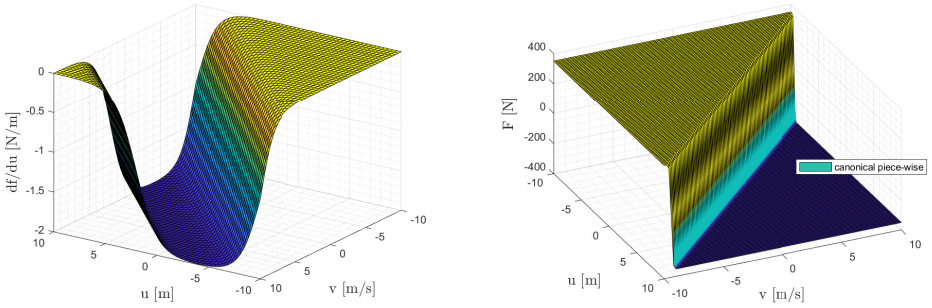

(a) First derivatives along position (b) Implemented control law

Figure 4: Derivatives and actual control law

The PD controller is no longer fully actuated, leading to saturation behavior and difficult parameters characterization. To overcome these troubles, it is suggested to start the modeling with a normal PD controller and then tune it with NASA guidelines. The control parameters required for this docking modeling are listed below.

SIMULATIONS

Here are presented the results of this modeling, the incoming velocity to the target is $v = 0.0368$ in the approaching direction. Different masses are simulated from 300 kg to 5000 kg and a first off-nominal characterization is provided by tilting the incoming spacecraft by 2 degrees with respect to the $\hat{x}$ axis, the incoming direction. The simulations constrain the bodies HCS SCS to keep relative alignment by imposing a total joint and addressing all the motion to the chaser vehicles. Further developments shall overcome

STATE	k_1 N/m	k_2 Ns/m	λ n.d.	F_{max} N	u_0 m	$\dot{u}_0$ m/s
EXTRACTION	2000	200	0.02	200	0.3	0
LUNGE	20	2000	0.02	67	0.4	0.1016
ATTENUATION	20000	50	0.02	356	0.05	0
ALIGNMENT	6000	5850	0.001	200	state machine	0
RETRACTION	$4 \cdot 10^6$	$4.4 \cdot 10^6$	0.0001	1200	state machine	0

Table 4: Control parameters

these limitations. Simulations are all presented with the same control parameters, to stress their performances and ranges, to follow the ultimate goal to develop a general tool. This shall change in a more detailed simulation where fine adjustment shall be performed, in this situation the customizability of the module and MBDyn, in general, allows a more precise control parameters definition.

The first two plots show the approaching direction in the nominal situation, simulating the mass of the system alone ($300kg$), from the point of view of the vehicle flying to the space station and from the relative displacement of the actuator. The results show a position profile that makes clear the full docking achievement. Simulating different weights with the same control can easily bring uncontrolled situations, fortunately, this has not happened, since the control is robust enough.

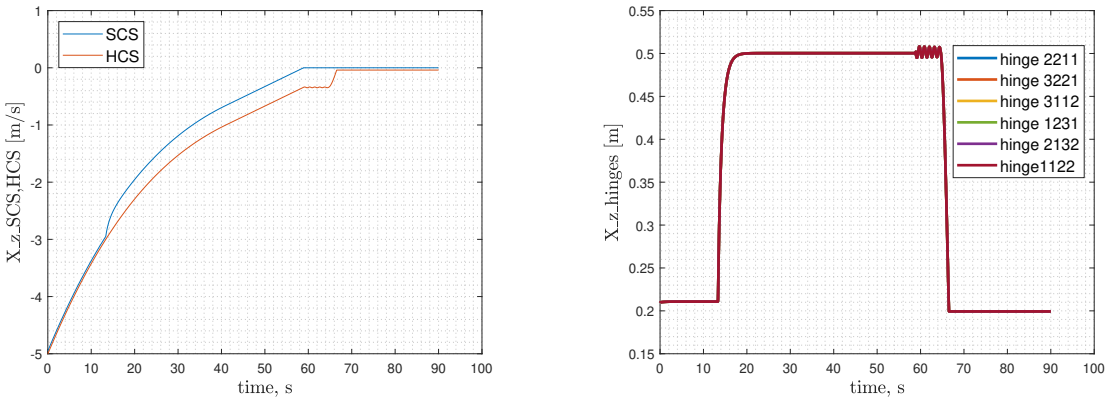

(a) HCS and SCS pos. along incoming axis (b) Relative motion of all actuators

Figure 5: Positions for nominal 300 kg simulation

Below are shown the actuators' control forces and relative velocities. Even if the forces are embedded with respect to the prescribed forces stated by NASA, it shall be pointed out that in this light configuration, forces oscillate a lot and it can become an issue to

overcome. Velocities are quite low everywhere, there are oscillations but they do not have a wide excursion.

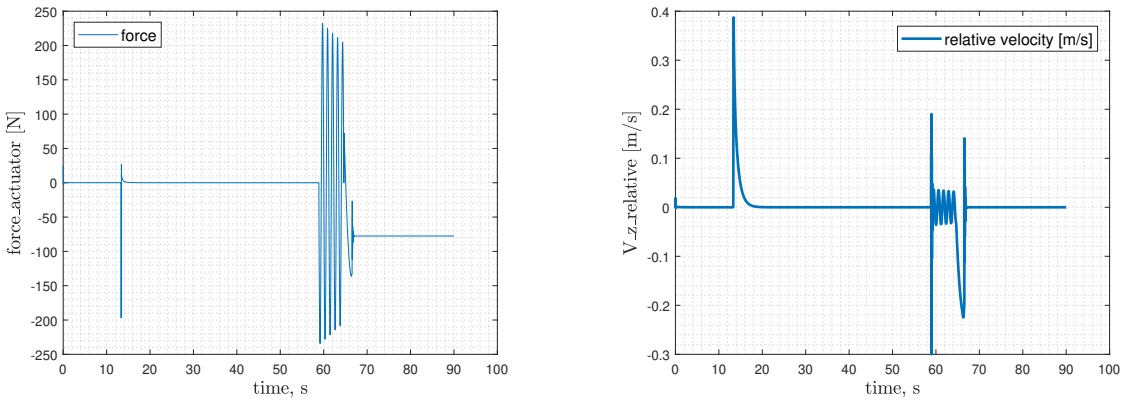

(a) Actuator force (b) Actuator relative velocity

Figure 6: Force and velocity for 300 kg nominal simulation

The off-nominal situation in general, with the plot of the positions, shows that even in this situation the simulation provides good results and the docking is achieved, and zoom over the attenuation mode is provided, it is an important moment where the system is highly stressed and differences between nominal and off-nominal are more visible.

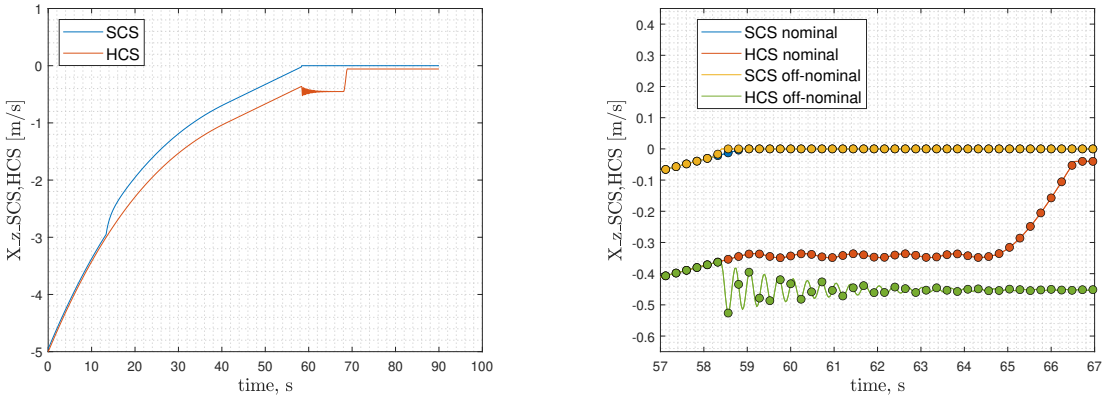

(a) 300 kg off-nominal HCS and SCS displ. (b) Zoom & comparison in atten. mode

Figure 7: Off-nominal general behavior and comparison with nominal simulation

The 5000 kg configuration is presented below, it is already in the off-nominal situation and without the constraint on the spacecraft path, increasing its generality. The plots still show the docking obtained. The comparison is with the off-nominal of 300 kg.

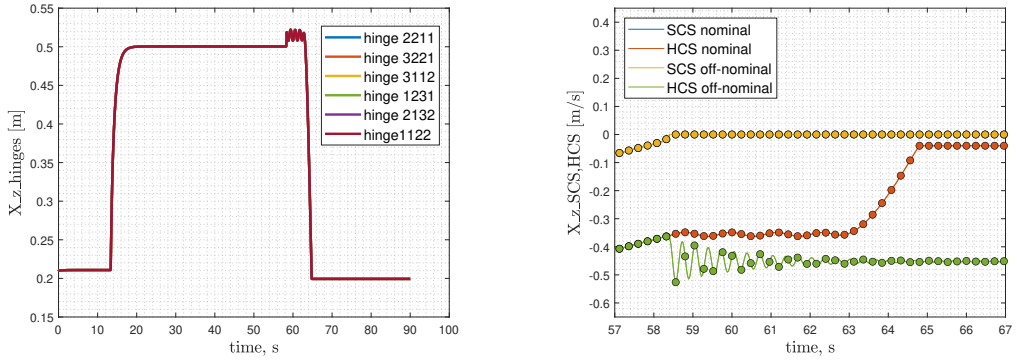

(a) Relative actuator displacements (b) Comparison between different masses

Figure 8: Off-nominal, 5000 kg simulation

CONCLUSIONS

Further analysis shall be addressed to let the presented system general enough to be implemented autonomously in different algorithms, here are presented some issues to be overcome in future works.

A more automatic system to set the control parameters should be defined since even if the work in this thesis makes the number of control parameters the fewest as possible while smoothing and respecting NASA guidelines for control, their number still does not allow for an easy way to select them.

The model and its simulations are still relatively simple. It is missing the full petal contact description, and the spacecraft's motion is still constrained to be nominal besides some tilting on the $\hat{x}$ axis that provides a first off-nominal. Overcoming these issues provides a more reliable tool for simulating control or determining navigation trajectories. The solution to these problems shall be recovered in a new control parameters characterization and in a more detailed contact description.

This work provides a first tool for analysis, with its computational velocity the motion can be simulated in a promising way for embedded analysis, it already simulates with some off-nominal. The NASA control laws are followed in their principal aspects while reducing their complexity still can be adopted for a preliminary analysis.

1 | Introduction

1.1. The Docking Problem

To successfully extend in-space capabilities, Rendezvous and Docking or Berthing (RVD/B) technology and techniques are used to resupply orbital platforms and stations, swap crews in orbital stations, repair spacecraft in orbit, retrieve and capture spacecraft to bring them back to Earth, and re-join orbiting vehicles from the ground, recalling Fehse's book [1].

The docking or berthing problem consists of the capture and mating of two objects, both in orbit at high-speed velocities, where both the dynamics of the spacecraft's complex bodies and the guidance, navigation, and control are critical to the mission's success, and any errors might be disastrous.

Berthing a spacecraft is the act of two spacecraft joining and sealing to one another while in Earth's orbit or deep space with the aid of a robotic arm. For berthing, a robotic arm guides a target ship to a certain spot as it comes in for its final approach.

Docking is the act of two spacecraft joining and sealing to one another while in Earth's orbit or deep space, with a Guidance Navigation and Control (GNC) system active until the first touch and with their robotic mating systems. Each spaceship has a docking system that is meant to catch the docking system of the other ship. One shall be in a passive mode and the other in an active mode, trying to catch the target with its robotic system. Astronauts can accomplish this task by docking manually, or the spacecraft's control systems, which are comprehensive in terms of sensors and navigation information, can do it automatically.

Historically, everything began with the Gemini mission on March 16, 1966, when Neil Armstrong and Dave Scott used a Gemini spacecraft to manually dock, this is the first-ever rendezvous and docking between two spacecraft. They docked with an unmanned Agena target spacecraft. As the Soviet vehicles Cosmos 186 and 188 docked on October 30, 1967, the first automatic RVD took place.

While the International Space Station (ISS) has been the primary application of RVD/B

technology during the first two decades of the twenty-first century, other rendezvous missions have occurred and will occur: those to service spacecraft in orbit (such as the Hubble Space Telescope or Mission Extension Vehicle, in future for the Webb Telescope), for active debris removal missions (like in Clearspace missions), to make happen complex planetary exploration (like for Apollo missions), or to return to the moon or other planets in a stable way (such as with Lunar Gateway Station).

From the point of view of navigation, both docking and berthing are made up of a series of maneuvers that lead up to the actual docking (or berthing). GNC aims to bring the active vehicle (the chaser) closer to the passive vehicle (the target) until contact is made. The chaser must be put in the right place, at the right speed, with the right attitude, and at the right angle rates.

Note that approaching a target must be under some constraints: the target spacecraft may set up keep-out zones, approach trajectory corridors, and hold points. The ground crew or target crew may need to give the chaser their clearance to continue at specific stages throughout the approach. If the chaser vehicle crashes into the target, the safety of the crew and the vehicle could be at risk if its dynamic states are greater than what is allowed by the approach trajectory.

Since in rendezvous ensuring that each system function is vital, both individually and collectively, and the real environment will only be present during the operative mission, it becomes crucial to define a proper simulation environment and model. It may be possible to model both the docking dynamics and control logic in the most embedded way between different fields such as Guidance Navigation and Control (GNC) design, Attitude Determination and Control System (ADCS) design, Multi-body System Dynamics design and Structures, and Mechanisms design.

1.2. State of the Art of Space Docking Methods

Currently, docking technique families may be roughly separated into androgynous systems and non-androgynous systems. Androgynous systems are used when the mission needs to be flexible and the payloads to share are voluminous. Non-androgynous systems are used when the spacecraft needs to, and can, be smaller.

The techniques for docking in space are different and have changed dramatically throughout time. Currently, NASA and its international partners have created the International Docking System Standard (IDSS) to regulate spacecraft docking. Spacecraft in orbit can be linked together by the IDSS using both mechanical and electrical connections to seal,

match up structures, send data, and transfer energy. That allows an international standardization aiming to open the docking to different missions and for different spacecraft. Not only that, the system is designed as androgynous such that there is no need to define a male or female system, and this allows to enlarge the flexibility and possibilities to dock in space and so reduce the intrinsic difficulties of interacting in the space environment.

Androgynous systems are useful because they let any spaceship with a docking port talk to any other spaceship with the same docking system. By doing so, the space agency may avoid having to equip half of its fleet with male ports and the other half with female ports.

To provide a standard interface for spacecraft to dock with one another, NASA, ESA, JAXA, and Roscosmos have negotiated the IDSS definition so that the International Docking Adapter (IDA) lets any spacecraft having an IDSS-compliant docking mechanism to be able to connect to the International Space Station (ISS).

Nowadays, IDSS-compliant systems are the NASA Docking System Block 1 (NDSB1) and the European International Berthing and Docking Mechanism (IBDM).

To be thorough, it is essential to mention that non-androgynous systems, which distinguish between male and female ports, are also employed. This is how early docking missions, like the Gemini mission, were made up until the Apollo-Soyuz docking mission in 1975, which used the Androgynous Peripheral Attach System (APAS). These docking systems are still in use because they are lightweight, small, and have simpler contact mechanics.

1.3. Thesis Purpose and Workflow

The goal of this thesis is to improve docking mission modeling by running simulations quickly enough to be used in GNC and ADCS optimization algorithms to take docking dynamics into account when figuring out trajectory, control, and cost. To accomplish this, the appropriate program must be chosen.

The docking system model is made in MBDyn and includes three-dimensional contact interactions, masses, inertias, and joints.

To meet the thesis aim, new modules or updates to already programmed modules are given and coded, making use of MBDyn's versatility and customizability. This work is about how to define control logic and state machines for actuation modes, how to turn on and off different joints based on simulation states, and how to define limited contact regions.

MBDyn is chosen for its flexibility, it allows modeling via lumping the characteristics of the dynamic bodies and relative constraints in their principal elements. In this way, it is possible to overcome the problem of rewriting the dynamic problem via Python or Matlab or directly in C++. This allows easier modeling modification in the future, moreover, the general integration schemes in the existing libraries do not necessarily guarantee the correct computational time for the problem, via MBDyn also this aspect can be overcome, without rewriting the correct integration scheme for this specific simulation. Still, MBDyn is general and allows modeling without rewriting from scratch the problem, but it does not imply discretizing the bodies, it is light enough to be chosen for the embedding capabilities.

Control logic is characterized as linear with saturations, which present certain issues with the smoothness of the control and may become an issue for simulation. This thesis attempts to solve this challenge by preserving the saturation behavior while smoothing the n-dimensional surface control function with the fewest new parameters.

The thesis achieved its results through different modeling phases:

1. modeling the Visiting Vehicle (VV) and docking multibody dynamics system;
2. modeling the Hosting Vehicle (HV) and docking multibody dynamics system;
3. modeling the actuation logic
4. modeling the interaction between the two systems;
5. to unify the preceding models

This effort to provide a tool capable of embedded simulations to enhance the forecast capability of the designer:

1. to generate more realistic simulations and, as a result, more exact predictions;
2. to decrease the number of iterations necessary between various field designers;
3. to enable research into non-nominal events and their implications;
4. to offer cost reductions by accounting for docking dynamics and loads in the algorithms.

2 | Fundamentals

2.1. Mission and System Description

The thesis models the system using data from existing systems such as NASA Docking System Block 1 (NDSB1) [7], which is compliant with the International Docking System Standard (IDSS) [2], and recovers this information and specification from the related documents.

The IDSS Interface Definition Document (IDD) describes the precise geometric mating interface and the required design stresses. The physical geometric interface criteria must be strictly followed to establish physical spacecraft mating compatibility. Both areas with clearly defined components and those with voids are included. The IDD also includes a set of common design requirements, including information about vehicle mass and docking beginning conditions, it sets some recommended design criteria that increase the possibility of successful docking between different spacecraft.

The IDSS IDD assumes a rendezvous phase before docking and a two-stage docking procedure. To synchronize their docking interfaces during the docking stage, an active docking vehicle is supposed to relatively navigate to the passive docking vehicle during the rendezvous stage. Meeting the docking system's Initial Contact Condition requirements allowed the rendezvous stage to be completed.

The docking phases can be separated into two parts: the first capture of docking vehicles and the second structural mating step. The Soft Capture System (SCS) handles the first, and the Hard Capture System (HCS) handles the second. During the initial capture phase, the active docking mechanism's SCS aligns with and latches to the passive docking mechanism stabilizing the newly linked spacecraft relative to each other. The soft capture mechanism then pulls the docking spacecraft together to begin the second step of docking, which is carried out by the HCS. The HCS provides structural latching and sealing to transfer structural loads between spacecraft and to establish a safe tunnel for personnel and cargo transfer operations. To guarantee the correct docking procedure, the docking process must be performed within a certain time frame.

Since the IDSS docking interface is totally androgynous around one axis, when docking, one interface must be defined in active mode, while the other stays retracted and secured in place in passive mode. The active interface controls the soft capture function and all sequences of docking until hard capture completion.

The SCS interface comprises a capture ring, guiding petals, mechanical latches, mechanical latch strikers, sensors, sensor strikers (the region on the mating interface's passive side that is meant to provide a contact surface for an active component on the active side) and the Linear Actuator System (LAS). The three petals on the SCS Ring provide rough alignment and matching with equivalent petals on the mating docking ring. Each Capture Latch is located in the middle of the petal, Capture Latch holds the two mating rings together during docking.

The HCS comprises an interface tunnel, 12 active/passive hook pairs on each side, dual concentric pressure seals, fine alignment guide pins and guide pin receptacles, sensors, sensor strikers, a separation system, and resource umbilicals.

The guiding petals are the first element to make contact during docking soft capture and this is referred to as first contact. The SCS acts, via petals and its geometry, to rectify the lateral and angular misalignment of the two opposing interfaces. Soft capture is defined as accomplished when the two capture rings' surfaces are in full contact: the active mechanical capture latches of the petals are fully engaged with the mechanical latch strikers on the opposing vehicle situated in the passive HCS.

The SCS then change its mode and start to align and retract the two vehicles to bring their hard capture interfaces into the hard capture range. Fine alignment is achieved with the use of SCS retraction and HCS guiding pins. The docking operation is complete when the mechanical hooks and resource umbilicals are fully engaged.

To actuate all the control logic and manage all the docking modes, NASA and Boeing defined the actuator system capable of accomplishing the tasks like the Soft Impact Mating and Attenuation Concept (SIMAC) as [8, 9] show. In the presence of reasonable initial relative misalignments and rates between the two rings, the linear actuator system moves the soft capture ring in a manner that forces alignment of the active ring to the passive ring, so that capture devices on the rings can trap the two rings together for a successful soft capture. Linear Actuator System is electrical and electrically driven.

The Linear Actuator System (LAS) consists of six Linear Actuators displaced in a Stewart platform fashion, and a control avionics box called the Linear Actuator Controller (LAC). LAS is in charge of controlling the SCS Ring throughout the soft capture.

LAS control logic defines that each of the six linear actuators from each other shall be independent, so there is no requirement for mechanical connectivity or closed-loop control between them. The shared information between actuators is to work in a series of operating modes, but they act independently to achieve the goal during that mode. Another characteristic is the load-limiting capability of each linear actuator: the load applied by each actuator is limited as stated for that mode. This last feature reduces the overall stress transferred by the soft capture ring on the passive ring and the structure behind it. The thesis deals with this logic requirement trying to avoid discontinuities in the commands.

The independence of the actuators decreases the amount of hardware like interconnections and sensors, decreasing weight and lowering complexity and risk, letting the overall reliability of the system increase.

The series of operating modes that LAS shall perform, with the linear actuators responding differently in each phase, include:

1. deploying the active soft capture ring from a "stowed" configuration to a "Ready to Capture" extended state;
2. executing a "lunge" maneuver of the soft capture ring to effect alignment and capture of the passive capture ring;
3. transitioning to an "attenuation" mode to remove remaining relative motion, executing an "alignment" mode to align the active and passive rings;
4. concluding with a "retraction" mode to bring the vehicles together.

The lunge docking operation demands the mechanism to deliver energy in the engaging direction while also complying with reactionary pressures after the docking ring contacts the mating alignment guide petals. The attenuation mode is in charge of dampening the motion between the newly connected structures, once the soft capture ring is locked in place. Thereafter the motion between the mass bodies is entirely attenuated, and the actuation system is in charge of motion control for precise alignment of the vehicles, allowing Hard Capture to be completed.

2.2. Relative Navigation

A rendezvous mission may be separated into several distinct phases: launch, phasing, far-range rendezvous, near-range rendezvous, and mating. During these phases, the kinematic and dynamic conditions that would eventually allow the chaser to link to the target

spacecraft should be shown, following Ankersen's work in [1, 15].

The rendezvous mission for thesis purposes can start when the chaser vehicle is placed in a stable orbit in the desired orbital plane at the end of the launch phase. The chaser vehicle is therefore an arbitrary phase angle behind the target, depending on the target's orbit characteristics and the actual launch. Generally being launched from Earth implies having a lower orbit, but it is not always the case.

To describe the motion of the arriving spacecraft with respect to the other it becomes convenient to maintain one of the spacecraft as a fixed point for relative navigation. The reference frame shall originate in the Center of Mass (CoM) of the target vehicle: target spacecraft's local orbital frame. The Hill equations (the equations of relative motion for circular orbits) are here shortly explained to understand the mathematical model to analyze the docking situation from the navigation point of view.

Given:

$\mathbf{F}_g$: gravitational force; G: universal gravitational constant; M: mass of the central body; m: mass of the spacecraft; $\mathbf{r}$: the radius vector and $r = ||\mathbf{r}||$; $\mu = GM$, planetary constant;

The dynamic equation for an object with mass subjected to a spherical gravitational field:

$$\mathbf{F}_g = -\mu \frac{m}{r^3}\mathbf{r} \tag{2.1}$$

Considering the relative displacement $\mathbf{s}$ between the target $\mathbf{r}_t$ and the chaser $\mathbf{r}_c$ vehicles: $\mathbf{s} = \mathbf{r}_c - \mathbf{r}_t$, it is easy to obtain with control/disturbances force $\mathbf{F}(\mathbf{r}, t)$ is:

$$m\ddot{\mathbf{s}} = \mathbf{F}_g(\mathbf{r}_c) - \mathbf{F}_g(\mathbf{r}_t) + \mathbf{F} \tag{2.2}$$

Linearizing the gravitational field contribution of the chaser around the target, with $\mathbf{f}_g(\mathbf{r}_c) = \mathbf{F}_g(\mathbf{r}_c)/m$ and $\mathbf{f}_g(\mathbf{r}_t) = \mathbf{F}_g(\mathbf{r}_t)/m$:

$$\mathbf{f}_g(\mathbf{r}_c) = \mathbf{f}_g(\mathbf{r}_t) + \left.\frac{\mathrm{d}\mathbf{f}_g(\mathbf{r})}{\mathrm{d}\mathbf{r}}\right|_{\mathbf{r}=\mathbf{r}_t} (\mathbf{r}_c - \mathbf{r}_t) \tag{2.3}$$

where:

$$\left.\frac{\mathrm{d}\mathbf{f}_g(\mathbf{r})}{\mathrm{d}\mathbf{r}}\right|_{\mathbf{r}=\mathbf{r}_t} = \mathbf{K}(\mathbf{r}) = \begin{bmatrix} 1-3\frac{r_x^2}{r_t^2} & 3\frac{r_x r_y}{r_t^2} & 3\frac{r_x r_z}{r_t^2} \\ 3\frac{r_x r_y}{r_t^2} & 1-3\frac{r_y^2}{r_t^2} & 3\frac{r_y r_z}{r_t^2} \\ 3\frac{r_x r_z}{r_t^2} & 3\frac{r_y r_z}{r_t^2} & 1-3\frac{r_z^2}{r_t^2} \end{bmatrix} \tag{2.4}$$

So the 2.2 becomes:

$$\ddot{\mathbf{s}} = -\frac{\mu}{r_t^3}\mathbf{K}\mathbf{s} + \frac{\mathbf{F}}{m} \tag{2.5}$$

To represent the chaser motion in the rotating target local orbital frame, recalling acceleration in the rotating target frame, given $\boldsymbol{\omega}$ rotating rate and $\mathbf{s}^*$ in the rotating frame, the 2.5 becomes:

$$\ddot{\mathbf{s}} = \frac{\mathrm{d}^2\mathbf{s}^*}{\mathrm{d}^2 t} + \boldsymbol{\omega} \times (\boldsymbol{\omega} \times \mathbf{s}^*) + 2\boldsymbol{\omega} \times \frac{\mathrm{d}\mathbf{s}^*}{\mathrm{d}t} + \frac{\mathrm{d}\boldsymbol{\omega}}{\mathrm{d}t} \times \mathbf{s}^* = -\frac{\mu}{r_t^3}\mathbf{K}\mathbf{s}^* + \frac{\mathbf{F}}{m} \tag{2.6}$$

In the hypothesis of circular orbits $\boldsymbol{\omega} = \sqrt{\frac{\mu}{r_t^3}}$ and $\frac{\mathrm{d}\boldsymbol{\omega}}{\mathrm{d}t} = \mathbf{0}$, the Hill's equations for the linearized relative dynamics can be obtained:

$$\begin{cases} \ddot{x} - 2\omega\dot{z} = \frac{1}{m}F_x \\ \ddot{y} + 2\omega y = \frac{1}{m}F_y \\ \ddot{z} - 2\omega\dot{x} - 3\omega^2 z = \frac{1}{m}F_z \end{cases} \tag{2.7}$$

This is the navigation framework of the spacecraft dynamics where to model and simulate the multibody dynamics of the docking interaction. The thesis works to simulate in this framework the design of docking phases, having into account the multibody dynamics of the systems.

Below the solution of Hill's equations after a $\Delta\mathbf{v}$, without any forcing terms (like after an impulsive maneuver), given $\mathbf{x}_0$, $\dot{\mathbf{x}}_0$ and t_0 in the relative reference frame:

$$\begin{cases} x(t) = \left(\dfrac{4\dot{x}_0}{\omega} - 6z_0\right)\sin(\omega(t-t_0)) - \dfrac{2\dot{z}_0}{\omega}\cos(\omega(t-t_0)) + (6\omega z_0 - 3\dot{x}_0)(t-t_0) + \left(x_0 + \dfrac{2\dot{z}_0}{\omega}\right) \\ y(t) = y_0\cos(\omega(t-t_0)) + \dfrac{\dot{y}_0}{\omega}\sin(\omega(t-t_0)) \\ z(t) = \left(\dfrac{2\dot{x}_0}{\omega} - 2z_0\right)\cos(\omega(t-t_0)) + \dfrac{\dot{z}_0}{\omega}\cos(\omega(t-t_0)) + \left(4z_0 + \dfrac{2\dot{x}_0}{\omega}\right) \end{cases} \tag{2.8}$$

2.3. Multibody System Dynamics

To allow a full comprehension of the framework a brief recap of the Multibody System Dynamics principal results is now presented, following the [16–18] references.

Starting from kinematics definition, given a body reference frame F^B, provide an origin point $\mathbf{B}$ and a basis B^*, given an inertial reference frame F^I, provides an origin point $\mathbf{O}$ and a basis I, the motion $\mathbf{r}(t)$ of a point $\mathbf{P}$ is so defined:

$$\mathbf{r}_P(t) = \mathbf{r}_B(t) + \mathbf{u}(t) = \mathbf{r}_B(t) + \mathbf{R}(t)\mathbf{u}^*(t) \tag{2.9}$$

where $\mathbf{u} = \mathbf{R}\mathbf{u}^*$ are the components of the position vector of point $\mathbf{P}$ with respect to point $\mathbf{P}$ resolved in basis I, meaning: $\mathbf{u}^* = \mathbf{R}^\top(\mathbf{r}_P - \mathbf{r}_B)$. The inertial velocity of $\mathbf{r}_P(t)$, $\mathbf{v}_P(t)$ becomes:

$$\mathbf{v}_P = \mathbf{v}_B + \dot{\mathbf{R}}\mathbf{u}^* + \mathbf{R}\dot{\mathbf{u}}^* = \mathbf{v}_B + \boldsymbol{\omega} \times (\mathbf{r}_P - \mathbf{r}_B) + \mathbf{R}\dot{\mathbf{u}}^* \tag{2.10}$$

The inertial acceleration $\mathbf{a}_P(t)$ becomes:

$$\mathbf{a}_P = \mathbf{a}_B + (\dot{\boldsymbol{\omega}} \times + \boldsymbol{\omega} \times \boldsymbol{\omega} \times)(\mathbf{r}_P - \mathbf{r}_B) + 2\boldsymbol{\omega} \times \mathbf{R}\dot{\mathbf{u}}^* + \mathbf{R}\ddot{\mathbf{u}}^* \tag{2.11}$$

Defined the triad with origin in $\mathbf{P}$, rotated by $\mathbf{R}_{P-B}$ relative to the rigid body, so the absolute orientation of the triad in $\mathbf{P}$:

$$\mathbf{R}_P = \mathbf{R}\mathbf{R}_{P-B} \tag{2.12}$$

The absolute angular velocity of the triad in **P**:

$$\boldsymbol{\omega}_P = \boldsymbol{\omega} + \mathbf{R}\boldsymbol{\omega}_{P-B} \tag{2.13}$$

The absolute angular acceleration of the triad in **P**:

$$\dot{\boldsymbol{\omega}}_P = \dot{\boldsymbol{\omega}} + \boldsymbol{\omega} \times \mathbf{R}\boldsymbol{\omega}_{P-B} + \mathbf{R}\dot{\boldsymbol{\omega}}_{P-B} \tag{2.14}$$

If point **P** belongs to the rigid body, the components of its position vector relative to point **B**, with respect to the body attached basis, are constant in time. This means to velocities and accelerations:

$$\begin{aligned} \mathbf{v}_P &= \mathbf{v}_B + \boldsymbol{\omega} \times (\mathbf{r}_P - \mathbf{r}_B) \\ \mathbf{a}_P &= \mathbf{a}_B + (\dot{\boldsymbol{\omega}} \times + \boldsymbol{\omega} \times \boldsymbol{\omega} \times)(\mathbf{r}_P - \mathbf{r}_B) \end{aligned} \tag{2.15}$$

Velocity and acceleration relations represent a constraint on the derivatives of the positions of two arbitrary points of the same rigid body.

Obtaining the general dynamical system for constrained bodies with n degrees of freedom can be done in various ways, here is presented a straightforward one, via Lagrange formulation and Hamilton's Principle.

Given a set of generalized coordinates, define the Lagrangian function L as the difference between the kinetic E_k and the potential E_p energy of a system, define the generalized non-conservative forces $\mathbf{Q_q}$ exploiting the virtual work of the remaining non-conservative force δW_{nc} , so:

$$\begin{aligned} L &= E_k - E_p \\ \mathbf{Q_q}\delta\mathbf{q} &= \delta W_{nc} \end{aligned} \tag{2.16}$$

Define the augmented Lagrangian function $L' = L - \boldsymbol{\lambda} \cdot \boldsymbol{\phi}$ with multipliers $\boldsymbol{\lambda}$ as generic coordinates and a set of kinematic constraints expressed as algebraic equations $\boldsymbol{\phi}(\mathbf{q}, t) = \mathbf{0}$.

Given the variation of the Lagrangian and plugging it in the Hamilton principle of least

action:

$$\delta L = \frac{\partial L}{\partial \mathbf{q}}^{\top} \delta \mathbf{q} + \frac{\partial L}{\partial \dot{\mathbf{q}}}^{\top} \delta \dot{\mathbf{q}} \tag{2.17}$$

$$\int_{t_1}^{t_2} \delta L + \delta W_{nc}\, dt = \int_{t_1}^{t_2} \frac{\partial L}{\partial \mathbf{q}}^{\top} \delta \mathbf{q} + \frac{\partial L}{\partial \dot{\mathbf{q}}}^{\top} \delta \dot{\mathbf{q}} + \delta W_{nc} dt = 0 \tag{2.18}$$

Integrating by parts, knowing from variational calculus that in the boundary the variation is null:

$$\int_{t_1}^{t_2} \frac{\partial L}{\partial \dot{\mathbf{q}}}^{\top} \delta \dot{\mathbf{q}}\, dt = -\int_{t_1}^{t_2} \frac{\mathrm{d}}{\mathrm{d}t} \frac{\partial L}{\partial \dot{\mathbf{q}}}^{\top} \delta \mathbf{q} dt + 0 \tag{2.19}$$

So:

$$\int_{t_1}^{t_2} \delta \mathbf{q} \Big(-\frac{\mathrm{d}}{\mathrm{d}t} \frac{\partial L}{\partial \dot{\mathbf{q}}}^{\top} + \frac{\partial L}{\partial \mathbf{q}}^{\top} + \mathbf{Q_q} \Big) dt = 0 \tag{2.20}$$

So:

$$\frac{\mathrm{d}}{\mathrm{d}t} \frac{\partial L}{\partial \dot{\mathbf{q}}}^{\top} - \frac{\partial L}{\partial \mathbf{q}}^{\top} = \mathbf{Q_q} \tag{2.21}$$

At this stage, one simply needs to apply the Lagrange formalism to the augmented Lagrangian function:

$$\begin{cases} \dfrac{\mathrm{d}}{\mathrm{d}t} \dfrac{\partial L'}{\partial \dot{\mathbf{q}}}^{\top} - \dfrac{\partial L'}{\partial \mathbf{q}}^{\top} = \mathbf{Q_q} \\ \dfrac{\mathrm{d}}{\mathrm{d}t} \dfrac{\partial L'}{\partial \dot{\boldsymbol{\lambda}}}^{\top} - \dfrac{\partial L'}{\partial \boldsymbol{\lambda}}^{\top} = \mathbf{0} \end{cases} \tag{2.22}$$

where $\mathbf{Q_q}$ now only represent the non-conservative generalized forces energetically conjugated to the coordinates $\mathbf{q}$, since the inertia and conservative contributions are already dealt with by the derivatives of the Lagrangian function. The resulting Lagrange equations of the first kind are:

$$\begin{cases} \dfrac{\mathrm{d}}{\mathrm{d}t}\dfrac{\partial L}{\partial \dot{\mathbf{q}}}^{\top} - \dfrac{\partial L}{\partial \mathbf{q}}^{\top} + \boldsymbol{\phi}_{/\mathbf{q}}^{\top}\boldsymbol{\lambda} = \mathbf{Q}_{\mathbf{q}} \\ \boldsymbol{\phi} = \mathbf{0} \end{cases} \tag{2.23}$$

From Lagrange's equations of the first kind, or any equivalent formulation, this system of Differential-Algebraic Equations (DAE) can be expressed in the form:

$$\begin{cases} \mathbf{M}(\mathbf{q})\ddot{\mathbf{q}} + \boldsymbol{\phi}_{/\mathbf{q}}^{\top}\boldsymbol{\lambda} = \mathbf{f}(\dot{\mathbf{q}}, \mathbf{q}, t) \\ \boldsymbol{\phi}(\mathbf{q}, t) = \mathbf{0} \end{cases} \tag{2.24}$$

$\mathbf{M}(\mathbf{q})$ is the inertia matrix, $\boldsymbol{\phi}_{/\mathbf{q}}^{\top}\boldsymbol{\lambda}$ the generalized constraint reaction forces, and vector $\mathbf{f}(\dot{\mathbf{q}}, \mathbf{q}, t)$ accounts for the remaining forces.

Considering also non-holonomic constraints equations $\boldsymbol{\psi}(\dot{\mathbf{q}}, \mathbf{q}, t) = \mathbf{0}$:

$$\begin{cases} \mathbf{M}(\mathbf{q})\ddot{\mathbf{q}} + \boldsymbol{\phi}_{/\mathbf{q}}^{\top}\boldsymbol{\lambda}_{\phi} + \boldsymbol{\psi}_{/\dot{\mathbf{q}}}^{\top}\boldsymbol{\lambda}_{\psi} = \mathbf{f}(\dot{\mathbf{q}}, \mathbf{q}, t) \\ \boldsymbol{\phi}(\mathbf{q}, t) = \mathbf{0} \\ \boldsymbol{\psi}(\dot{\mathbf{q}}, \mathbf{q}, t) = \mathbf{0} \end{cases} \tag{2.25}$$

Euler's equations are an interesting example of the so-formulated dynamic system, they describe the motion of an unconstrained, rotating, rigid body, and an immediate application is the attitude dynamic of an orbiting spacecraft, like the ones for a docking mission. Recalling the kinematic and referring to the body reference frame F^B:

$$\mathbf{m}_{cm}^{*} = \mathbf{J}_{cm}\dot{\boldsymbol{\omega}} + \boldsymbol{\omega} \times \mathbf{J}_{cm}\boldsymbol{\omega} \tag{2.26}$$

where $\mathbf{m}_{cm}^{*} = \mathbf{R}^{\top}\mathbf{m}_{cm}$ is the sum of the externally applied moments computed with respect to the center of mass and resolved in a principal body basis. Explicitly:

$$\begin{cases} J_{cm_1}\omega_1 + (J_{cm_2} - J_{cm_3})\omega_2\omega_3 = m_{cm_1}^{*} \\ J_{cm_2}\omega_2 + (J_{cm_3} - J_{cm_1})\omega_3\omega_1 = m_{cm_2}^{*} \\ J_{cm_3}\omega_3 + (J_{cm_1} - J_{cm_2})\omega_1\omega_2 = m_{cm_3}^{*} \end{cases} \tag{2.27}$$

Having defined in the previous chapter the dynamics for the Center of Mass of a spacecraft subjected to a spherically symmetric gravitational field, having specialized it in a proximity relative navigation situation, having defined here its rotational dynamics, considering

it as a rigid body and having stated the general constrained multibody dynamics system, the framework for the mechanical and dynamical analysis for a docking mission is set.

2.4. The MBDyn Software

MBDyn [3, 4] is the first and one of the few full-featured free general-purpose Multibody Dynamics analysis software. It has been developed at the Dipartimento di Scienze e Tecnologie Aerospaziali (formerly Dipartimento di Ingegneria Aerospaziale) of the University "Politecnico di Milano", Italy. Here are shortly listed its fundamental characteristics and traits.

MBDyn features the integrated multidisciplinary simulation of multibody, multiphysics systems, including nonlinear mechanics of rigid and flexible bodies (geometrically exact & composite-ready beam and shell finite elements, component mode synthesis elements, lumped elements) subjected to kinematic constraints, along with smart materials, electric networks, active control, hydraulic networks, and essential fixed-wing and rotorcraft aerodynamics.

MBDyn simulates the behavior of heterogeneous mechanical, aeroservoelastic systems based on first principles equations.

MBDyn can be easily coupled to external solvers for co-simulation of multiphysics problems, e.g. Computational Fluid Dynamics (CFD), terra-dynamics, block-diagram solvers like Scicos, Scicoslab, and Simulink, using a simple C, C++ or Python peer-side API.

MBDyn is being actively developed and used in the aerospace (aircraft, helicopters, tilt rotors, spacecraft), wind energy (wind turbines), automotive (cars, trucks) and mechatronic fields (industrial robots, parallel robots, micro aerial vehicles (MAV)) for the analysis and simulation of the dynamics of complex systems.

Run-time loading of user-defined modules is leveraged to let users extend the feature library (elements, drives, constitutive laws, and more).

On GNU/Linux, real-time execution is supported under the Real-Time Application Interface, RTAI, and POSIX tight scheduling.

About the integration scheme adopted in MBDyn, starting from a generic system of implicit Differential–Algebraic Equations (DAE)

$$\mathbf{r}(\dot{\mathbf{q}}, \mathbf{q}, t) = \mathbf{0} \tag{2.28}$$

A prediction–correction approach is used to solve implicit A/L stable linear multistep integration schemes, where a perturbation of the integration scheme is used in the iterative solution of the correction phase:

$$\begin{cases} \mathbf{q}_k = \sum_{i=1:2} a_i \, \mathbf{q}_{k-i} + h \sum_{i=0:2} b_i \, \dot{\mathbf{q}}_{k-i} \\ \delta\mathbf{q}_k = h \, b_0 \, \delta\dot{\mathbf{q}}_k \\ (hb_0\mathbf{r}_{/\mathbf{q}} + \mathbf{r}_{/\dot{\mathbf{q}}})\delta\mathbf{q} = -\mathbf{r}(\dot{\mathbf{q}}_k^{(j)}, \mathbf{q}_k^{(j)}, t) \\ \dot{\mathbf{q}}_k^{(j+1)} = \dot{\mathbf{q}}_k^{(j)} + \delta\dot{\mathbf{q}}_k \\ \mathbf{q}_k^{(j+1)} = \mathbf{q}_k^{(j)} + hb_0\delta\mathbf{q}_k \end{cases} \tag{2.29}$$

The linearization of the already stated constrained multibody dynamic problem, after scaling is:

$$\begin{bmatrix} \mathbf{M} & -hb_0\mathbf{I} & \mathbf{0} & \mathbf{0} \\ -(hb_0\mathbf{f}_{/\mathbf{q}} + \mathbf{f}_{/\dot{\mathbf{q}}}) & \mathbf{I} & \boldsymbol{\phi}_{/\boldsymbol{q}}^{\top} & \boldsymbol{\psi}_{/\dot{\boldsymbol{q}}}^{\top} \\ \boldsymbol{\phi}_{/\boldsymbol{q}} & \mathbf{0} & \mathbf{0} & \mathbf{0} \\ \boldsymbol{\psi}_{/\dot{\boldsymbol{q}}} & \mathbf{0} & \mathbf{0} & \mathbf{0} \end{bmatrix} \begin{bmatrix} \delta\dot{\mathbf{x}} \\ \delta\dot{\boldsymbol{\beta}} \\ \delta\boldsymbol{\lambda}_{\phi} \\ \delta\boldsymbol{\lambda}_{\psi} \end{bmatrix} = \mathbf{RHS} \tag{2.30}$$

It is important now to emphasize the points that lead to the MBDyn selection.

First of all for the co-simulation capability to perform a cooperative task among multiple peers, exchanging information required by each task to complete the analysis, because it becomes critical if the presented docking system modelization is integrated into other algorithms such as attitude control or optimal guidance to complete the docking mission.

Next, elements, drives, constitutive laws, and other aspects are customizable and saved in modules, which correlate their name with a pointer to a functional object that instantiates an entity of the provided kind. As run-time loadable modules, entities of various sorts may be implemented.

These two aspects, among others, let this software well-suited for the goals of this thesis work, although in terms of contact simulation, the otherwise excellent core multibody library falls behind competing algorithms, and contact detection and modeling present capabilities are limited. For this reason, the thesis has to deal with and overcome this issue, but it is critical to emphasize that the types of interactions to simulate are such that MBDyn can still deal with them effectively.

2.5. Impacts Dynamics

Docking dynamics implies the interaction between the mating systems via mechanical contacts, so impact dynamics shall be covered in order to better understand the physics underlying and the small changes in the MBDyn contact module code to implement better contact characterization.

Following the reference of [6]. A contact force can be decomposed into normal and tangential components to the shared tangent plane. Contact forces for solid bodies result from the local deformation of the colliding bodies; these forces and deformations maintain compatibility of displacements in the contact region, preventing interpenetration or overlap of the bodies. Tangential forces, such as friction, might occur if the bodies are rough and there is sliding in the contact region.

The interaction forces (other than friction) in an inelastic collision are non-conservative, resulting in a loss of kinetic energy as a result of the cycle of compression and restitution. Energy loss can occur as a result of irreversible elastic-plastic material behavior, rate-dependent material behavior, or elastic waves trapped between the separating entities.

In a rigid body impact, deformations are negligibly tiny and the impact period shall be regarded as instantaneous. The velocities of the colliding bodies fluctuate during this instantaneous impact, but there is no change in configuration; hence, inertia characteristics stay fixed. Two colliding bodies usually make their first contact at a shared coincident point known as contact point. If at least one of the bodies has a topologically smooth surface at the contact point, exists a plane tangent to this surface. If both bodies are convex and the surfaces have continuous curvature near the contact point, then they share a tangent plane. The contact force and relative velocity changes at contact point will be resolved into normal and tangential components to the common tangent plane.

Unless the impact speed is exceedingly low, energy is lost in a collision. Whatever the reason, it leads to a relationship between the normal component of contact force and compression. This dissipation causes less compliance during unloading (restitution) than was present during loading (compression), resulting in hysteresis in the force-deflection relation. The integral of the loading curve is the kinetic energy of relative motion that is transferred to the internal energy of deformation during loading. The integral of the unloading curve, on the other hand, is the elastic strain energy released from the deforming region during the restitution.

The contact force is responsible for these energy changes. If changes in relative velocity are obtained as a function of normal impulse the work done by the reaction force may be

simply estimated for the individual phases of compression and restitution.

The most basic model for representing force F_N created at the surfaces of two bodies in contact is a parallel spring-damper element. The model is known as the Kelvin-Voigt model, defining k_{el} elastic coefficient, c_{dam} damping coefficient, Δx relative displacement and $\dot{x}$ displacement rate, following [5, 19]:

$$F_N = k_{el}\Delta x + c_{dam}\dot{x} \tag{2.31}$$

A way to estimate the k_{el}, given the geometrical and material properties R_i, ν and E of the two bodies 1 and 2 can be recovered in:

$$\begin{aligned} \sigma_i &= \frac{1-\nu^2}{E} \\ k_{el} &= \frac{4}{3(\sigma_1+\sigma_2)}\sqrt{R_1} \end{aligned} \tag{2.32}$$

Note that it is not always correct estimate in this way k_{el}, so that this parameter, the restitution coefficient e_{res} and the exponent n shall be recovered experimentally.

The dissipation coefficient estimation is provided by exploiting Lankarani-Nikravesh or Flores et al. formulas, given e_{res} restitution coefficient and n exponent estimation, the reaction force in MBDyn is computed:

$$\begin{aligned} F_{react} &= k_{el}\Delta x^n\left(1+\frac{8}{5}\frac{1-e_{res}}{e_{res}\dot{x}^-}\right)\dot{x}; \quad \text{Flores et al.} \\ F_{react} &= k_{el}\Delta x^n\left(1+\frac{3}{4}\frac{1-e_{res}^2}{\dot{x}^-}\right)\dot{x}; \quad \text{Lankarani} - \text{Nikravesh} \end{aligned} \tag{2.33}$$

Note that some approximation and estimation over the parameters unknown can be done like the exponent n can be set to $3/2$ in cases where there is a parabolic distribution of contact stresses, in order to have an initial guess or recover the Hunt and Crossley estimation for the restitution coefficient for materials with a linear elastic range and for velocities not exceeding 0.5 $[m/s]$.

3 | Multibody Model

3.1. Geometry and Bodies Model

Here are presented the current IDSS IDD guidelines for materials and mass properties for the docking system and spacecraft. This chapter describes how the physical system is condensed in its principal features for the MBDyn modelization [2, 7].

The system is divided into three body elements, each one with its own material, mass, and inertia properties: International Space Station -Hosting Vehicle (HV)- comprehensive of the docking system, approaching spacecraft -Visiting Vehicle (VV)- comprehensive of the Hard Capture System (HCS), and the Visiting Vehicle Soft Capture System (SCS).

In MBDyn, an element refers to a physical component that is modeled within a multibody system. These elements can represent a wide range of physical components, including rigid bodies, flexible bodies, joints, springs, dampers, and actuators. Each element has its own set of properties and parameters that describe its behavior within the system. For example, a rigid body element may have properties such as mass, inertia, and geometry, while a joint element may have parameters that define its range of motion and stiffness.

The body element describes a lumped rigid body when connected to a regular, 6-degree-of-freedom structural node, or a point mass when connected to a rotation-less, 3-degree-of-freedom structural node.

MBDyn defines the Structural nodes, they can have *6* degrees of freedom (position and orientation), and thus describe the kinematics of rigid-body motion in space, or *3* degrees of freedom (position) and thus describe the kinematics of point mass motion in space. The stated three bodies are the dynamic nodes with inertia, so they provide linear and angular momenta degrees of freedom and automatically generate the so-called automatic structural elements like body elements.

Each body is attached to a node, with the possibility to define an offset between the body center of mass and the node displacement, in this modelization the spacecraft node and the HCS node overlap.

Moreover, in the modelization, it is useful to visualize different points in the geometry, so the dummy structural node has been added to ease the visualization of the kinematics of arbitrary points of the system during the simulation. It does not provide any degrees of freedom, and it must be attached to another node. They are used to visualize all the actuators' hinges the striker and latches displacements. There are *18* dummy nodes in the model.

The spacecraft selected for the simulation is the **IDSS - 5T** tabulated. The modeling was made hierarchically trying to resemble the design workflow described by Moog for the actuators' tests [20]. Starting simulating alone the single actuator and then wrapping around the overall system and spacecraft.

NDSB1	Guide Petal	SCS Ring	HCS Plane
Material	$7075-T7351$	"	2219-Al
density $[g/cc]$	2.81	"	2.84
Modulus E $[GPa]$	72	"	73.1
Poisson Ratio	0.33	"	"
Shear Modulus $[GPa]$	26.9	"	27.0
Yield Strength T_y $[MPa]$	434	"	350

Table 3.1: NDSB1 Materials Properties

Vehicles	I_{xx} $[kg \cdot m^2]$	I_{yy} $[kg \cdot m^2]$	I_{zz} $[kg \cdot m^2]$
IDSS - 25T	$70 \cdot 10^3$	$169 \cdot 10^3$	$169 \cdot 10^3$
IDSS - 20T	$55 \cdot 10^3$	$135 \cdot 10^3$	$135 \cdot 10^3$
IDSS - 15T	$41 \cdot 10^3$	$71 \cdot 10^3$	$71 \cdot 10^3$
IDSS - 10T	$17 \cdot 10^3$	$42 \cdot 10^3$	$42 \cdot 10^3$
IDSS - 5T	$34 \cdot 10^3$	$18 \cdot 10^3$	$18 \cdot 10^3$
SCS - 40kg	12.67	6.42	6.42
HCS - 300kg	579.4	450	452

Table 3.2: Visiting Vehicles Mass Properties

Vehicles	X $[m]$	Y $[m]$	Z $[m]$
IDSS - 25T	5.4	0	0
IDSS - 20T	4.3	0	0
IDSS - 15T	4.1	0	0
IDSS - 10T	3.5	0	0
IDSS - 5T	2.3	0	0
SCS	0.015	0	0
HCS	0.165	0.356	0.0045

Table 3.3: Coordinate of the Capture System Mating Plane Center

3.2. Joints Model Definition

In MBDyn [3, 4], a joint is an element that connects two or more rigid bodies within a multi-body system, allowing them to move relative to each other in a prescribed way. Joints are used to model the interactions between different parts of a mechanical system. There are several types of joints available in MBDyn, each with its own set of parameters that define its behavior. These parameters include the joint's range of motion, stiffness, damping, friction, and other characteristics that determine how the joint behaves as the system moves over time.

Joints may have internal degrees of freedom (the reaction forces) when they introduce kinematic constraints in form of algebraic relationships between the coordinates of the nodes they connect. Joints that introduce configuration-dependent forces are flexible joints.

By defining the properties of each joint element, and combining them together with the other elements, such as springs, dampers, actuators, and bodies the system can be fully described. The joint elements used are all total joints and rods.

The total joint element allows arbitrarily constraining specific components of the relative position and orientation of two nodes. The value of the constrained components of the relative position and orientation can be imposed by means of drives. As such, this element allows mimicking the behavior of most ideal constraints that connect two nodes.

This element is particularly useful when modeling complex mechanical systems where ideal constraints are required, since using drives the value of the constrained components of the relative position and orientation can be imposed, allowing for precise control over the motion of the connected bodies.

The rod element represents a force between two nodes that depends on the relative position and velocity of two points, each rigidly attached to a structural node. The direction of the force is also based on the relative position of the points: it is the line that passes through them. If no offset is defined, the points are the nodes themselves.

The model present *15* joint elements:

- *6* rods between HCS and SCS nodes, they model the linear actuator system (LAS);
- driven total joint between SCS ISS nodes, it performs the clamp when the mating systems are close enough so that the latches and strikers can impose a constrain along the motion axis;
- driven total joint between HCS ISS nodes, it performs the clamp when the mating systems are close enough so that the HCS active and passive hooks can constrain the capture system;
- driven total joint on HCS node imposes the velocity simulating the Guidance, Navigation, and Control (GNC) system;
- total joint between HCS SCS nodes, this imposes a slider between the HCS and SCS, it is then deleted, it is used for preliminary settings to reduce modelization uncertainties;
- total joint between HCS ISS nodes, this imposes a slider between the HCS and SCS, it is then deleted, it is used for preliminary settings to reduce modelization uncertainties;
- total joint on ISS, it clamps the ISS and can be deleted, in a first approximation ISS is not free to move;

Rods are the actuation elements and they provide the control logic to the docking system, such elements can be driven from user-defined modules, and that opportunity is exploited with a specific docking module with the state machine and control logic, following NASA guidelines.

Rods are displaced in a Steward platform fashion with 3 couples of hinges on SCS and 3 couples of mirrored hinges on HCS. The following table describes their relative positions with respect SCS and HCS centers with $\hat{x}$ direction along the motion line.

Hinge	x [m]	y [m]	z [m]
SCS_{11}	-0.06	0.04	-0.57
SCS_{12}	-0.06	-0.04	-0.57
SCS_{21}	-0.06	-0.51	0.25
SCS_{22}	-0.06	-0.48	0.32
SCS_{31}	-0.06	0.48	0.32
SCS_{32}	-0.06	0.51	0.25
HCS_{11}	-0.22	-0.04	0.57
HCS_{12}	-0.22	0.04	0.57
HCS_{21}	-0.22	0.51	-0.25
HCS_{22}	-0.22	0.48	-0.32
HCS_{31}	-0.22	-0.48	-0.32
HCS_{32}	-0.22	-0.51	-0.25

Table 3.4: Rod hinge displacements.

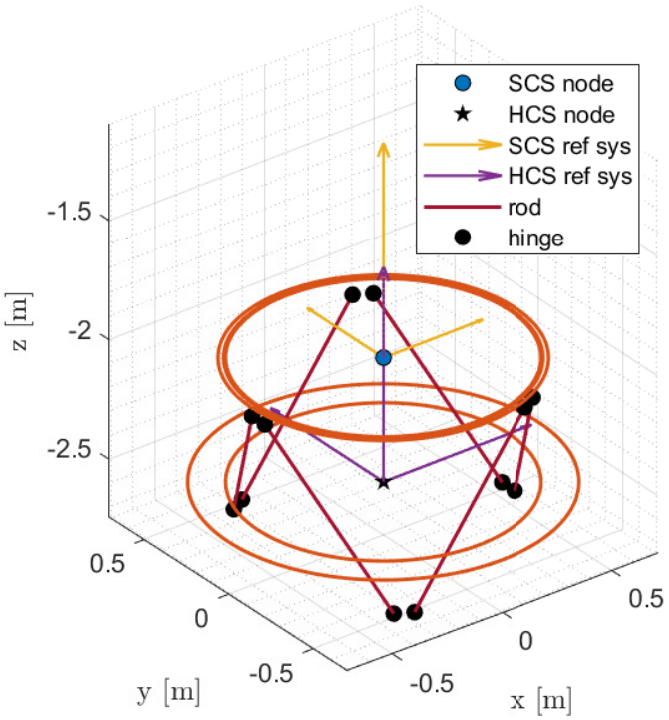

Figure 3.1: Geometry of the Docking System

3.3. Contacts Model

To model the contacts, still, joint elements are used, as can be recalled from the contact dynamics section they can be implemented in a constrained multibody problem as additional constraints on the dynamics.

The thesis deal with the modelization using and slightly modifying the module Cont-Contact already implemented. The adjustments now enable dealing with finite contact areas, as illustrated by a bouncing ball example: now, if the ball bounces at an angle with respect to the normal of the tangent plane, the outgoing velocity and angle can be significant enough to depart the region and allow the ball to fall freely in a parabolic path.

The regions in the mating systems where the contact can occur are the edges of petals and the latches and strikers spots. Here are reported the positions of the centers of the petals' edges and strikers and latches locations.

Hinge	x [m]	y [m]	z [m]
SCS_{11}	0.088	0.155	-0.393
SCS_{12}	0.088	-0.155	-0.393
SCS_{21}	0.088	-0.418	0.063
SCS_{22}	0.088	-0.263	0.330
SCS_{31}	0.088	0.263	0.330
SCS_{32}	0.088	0.418	0.063
ISS_{11}	-0.088	-0.155	0.393
ISS_{12}	-0.088	0.155	0.393
ISS_{21}	-0.088	0.418	-0.063
ISS_{22}	-0.088	0.263	-0.330
ISS_{31}	-0.088	-0.263	-0.330
ISS_{32}	-0.088	0.418	0.063
SCS Latch 1	0.06	0	-0.434
SCS Latch 2	0.06	-0.376	0.217
SCS Latch 3	0.06	0.376	0.217
ISS Striker 1	0.063	0	-0.434
ISS Striker 2	0.063	-0.376	0.217
ISS Striker 3	0.063	0.376	0.217

Table 3.5: Main Contact Points Displacement.

Given the dimensions of the edge limiting the contact area $a = 0.3[m]$ and $b = 0.011[m]$, tabulated below the orientations of each area, the contacts are geometrically well defined. The dimensions on the edges enforce the minimum number of contact points to avoid free penetration: *30* for each edge for a total of *180* contact points and relative contact joint.

Hinge	$\hat{v}_x$ [m]	$\hat{v}_y$ [m]	$\hat{v}_z$ [m]
ISS_{11}	$\begin{bmatrix} -0.599 \\ 0.708 \\ -0.374 \end{bmatrix}$	$\begin{bmatrix} -0.551 \\ -0.025 \\ 0.834 \end{bmatrix}$	$\hat{v}_x \times \hat{v}_y\|_{ISS_{11}}$
ISS_{12}	$\begin{bmatrix} -0.599 \\ -0.708 \\ -0.374 \end{bmatrix}$	$\begin{bmatrix} 0.552 \\ 0.026 \\ -0.834 \end{bmatrix}$	$\hat{v}_x \times \hat{v}_y\|_{ISS_{12}}$
ISS_{21}	$\begin{bmatrix} -0.599 \\ -0.678 \\ -0.426 \end{bmatrix}$	$\begin{bmatrix} -0.552 \\ 0.735 \\ -0.394 \end{bmatrix}$	$\hat{v}_x \times \hat{v}_y\|_{ISS_{21}}$
ISS_{22}	$\begin{bmatrix} -0.599 \\ 0.030 \\ 0.800 \end{bmatrix}$	$\begin{bmatrix} 0.552 \\ -0.734 \\ 0.394 \end{bmatrix}$	$\hat{v}_x \times \hat{v}_y\|_{ISS_{22}}$
ISS_{31}	$\begin{bmatrix} -0.599 \\ -0.030 \\ 0.800 \end{bmatrix}$	$\begin{bmatrix} -0.552 \\ -0.709 \\ -0.439 \end{bmatrix}$	$\hat{v}_x \times \hat{v}_y\|_{ISS_{31}}$
ISS_{32}	$\begin{bmatrix} -0.599 \\ 0.678 \\ -0.426 \end{bmatrix}$	$\begin{bmatrix} 0.552 \\ 0.709 \\ 0.439 \end{bmatrix}$	$\hat{v}_x \times \hat{v}_y\|_{ISS_{32}}$

Table 3.6: versors for the faces orientation.

Two kinds of contact are used in the modelization, the latches work when the rough alignment given by the petals is imposed, so the contact is provided by driving a rod joint element between the latch and striker, on the other hand, the contact between the petals is characterized by driving the deformable displacement joint.

The deformable displacement joint implements a configuration-dependent force that is exchanged between two points associated with two nodes with an offset. The force may depend, by way of a generic 3D constitutive law, on the relative position and velocity of the two points.

The contacts module requires the characterization of its parameters to model the situation,

in particular, it asks for formulation (Flores et al., Lankrani-Nikravesh, Hunt Crossley) restitution coefficient e_{res}, stiffness k_{el}, exponent n:

- formulation: Flores (et al.)
- $e_{res} = 0.6$;
- $k_{el} = 2e3$;
- $n = 1.5$;

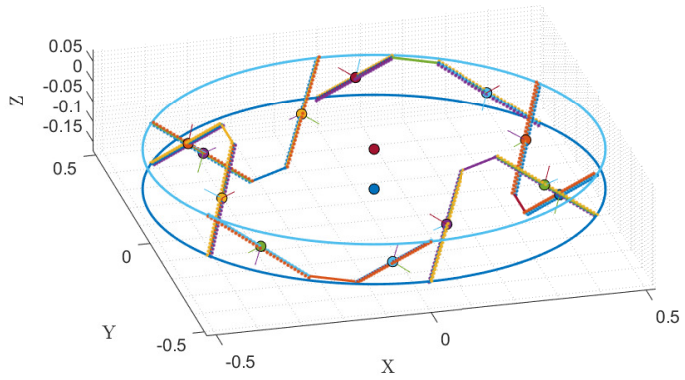

Figure 3.2: Contact Nodes Nominal Displacement

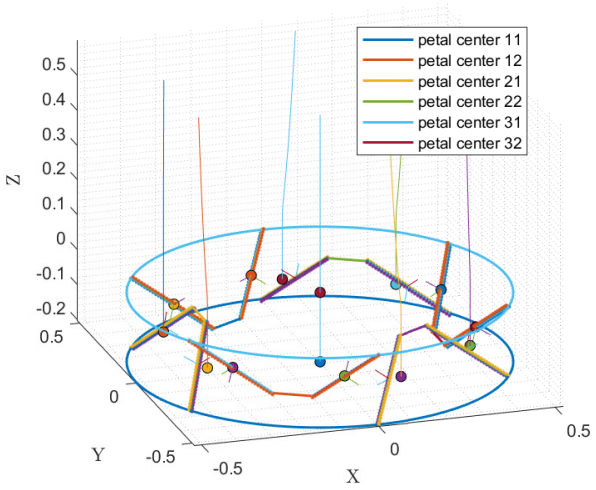

Figure 3.3: Contact Nodes Off-Nominal Interaction

4 | States and Control

4.1. State Machine Definition

The docking system presented and modeled by this thesis tries to simulate the NASA Docking System Block 1 (NDSB1) since it is the standardized docking system developed by NASA for use in various space missions. It is designed to allow spacecraft to dock autonomously with other vehicles or space stations, to accomplish this mission, a different control logic managed by a state machine shall be defined with the state machine itself.

In control theory, a "state machine" is a model that represents a system's behavior as a series of states and transitions between those states. It consists of a set of states that a system can be in and a set of events or inputs that cause the system to transition from one state to another. Each state represents a certain condition or way the system works, and the changes that happen between states show how the system's behavior or the way it works changes in response to outside stimuli.

The behavior of a state machine is defined by a set of rules or logic that determine which state the system should be in based on its current state and the inputs it receives.

The modes or states defined by the state machine are described in NASA documentation; they follow the phases that the docking situation imposed, and they are managed by the Linear Actuator System (LAS) [8, 9].

The aforementioned defined modes are:

1. INITIAL;
2. EXTRACTION;
3. LUNGE;
4. ATTENUATION;
5. ALIGNMENT;
6. RETRACTION;

7. STRUCTURAL MATING.

The ring is placed in a ready-to-capture position when it is first turned on, and its position is actively controlled until the first contact with the mating adapter is detected. These first two operations need the actuators to regulate the position of an unloaded ring.

The lunge mode causes the active soft capture ring to stretch in order to line up with and capture the passive soft capture ring. To do this, the six linear actuators are all told to lengthen at the same time at a set rate as soon as the active and passive soft capture rings come into contact. After being told what to do, each linear actuator works independently of the others and keeps going until capture is made.

As the rings are pulled toward each other along their axes, the geometry of the active and passive soft capture rings and their surrounding petals causes the rings to physically line up and eventually catch. To do this, certain linear actuators must extend to a greater length than others in order to force the active soft capture ring into a roughly linear and angular position that matches the passive soft capture ring.

The attenuation mode is initiated after the effective capture of the passive ring by the active ring during the lunge mode. At this moment, there is still relative motion between the chasing and target vehicles, and the goal is to stop all relative motion. The LAS does this by telling each linear actuator to stop moving and instead hold its last measured position, fight the incoming residual velocity up to a certain force threshold, and then start slipping with the maximum force allowed.

The align mode instructs the actuators to extend or retract to a specified length, causing the soft capture ring, and consequently the passive capture ring, to line up with the tunnel. This mode prepares the passive capture ring to be brought to the tunnel interface so that the HCS may make a hard connection between the two vehicles.

The retract mode tells the actuators to pull back at the same time from the end of the aligned mode state to a length that is long enough to bring the active and passive halves of the hard capture system close enough together to form a rigid structural connection. This procedure needs some position precision requirements on the actuator. There is still a desire to restrict the interface loads during actuator motion in both the retraction and alignment modes.

The conditions to trigger the state change are stated below, for each transition, it is required to be in the previous state to have a sequential ordering.

- The condition to pass from INITIAL to EXTRACTION mode is that the space-craft overcome a threshold distance, in this simulation, the triggering distance is

$d^{sc}_{extraction} < 3[m]$.

- Any contact between the docking system is required to transition from extraction to lunge mode. This implies accounting for any of the contact joints aforementioned, $\sum_i F_{cont_i} > 0$.
- The condition to pass from LUNGE to ATTENUATION mode: each latch is engaged to its striker within a certain tolerance, such that $||\mathbf{x}_{latch_i} - \mathbf{x}_{striker_i}|| < tol$, where $tol = 0.0005[m]$.
- The condition to pass from ATTENUATION to ALIGNMENT mode is that the spacecraft's kinetic energy is below a tolerance, $E^{SC}_{kin} < tol$, where $tol = 0.001$.
- The condition to pass from ALIGNMENT to RETRACTION mode is that each actuator length l_{LAS_i} is at the prescribed elongation l_{target} within a strict tolerance, $|l_{LAS_i} - l_{target}| < tol$, where $tol = 0.01[m]$.
- The condition to pass from RETRACTION to STRUCTURAL MATING mode is that the elongation of LAS is small enough to allow structural hooks engagement, such that $|l_{LAS_i} - l^{SM}_{target}| < tol$ with $l^{SM}_{target} = 0.2[m]$ and $tol = 0.001[m]$

In order to manage all the states and control laws, a new module written in C++ for MBDyn that fully handles that is provided, This modelization part also required the definition of a new driver that can drive joints and their turning on and off.

4.2. Control Logic

The thesis tries to follow NASA rules for both the state triggers and the control logic. For example, during a single mode, each linear actuator acts independently of the others, but when the mode changes, the transition should command coordinating all the LAS together.

The LAS has been developed as an actuation system with as little sensor feedback as possible. This made the system much smaller and, more importantly, made it more reliable by getting rid of potential points of failure. According to the design principle that "a component that is not there cannot fail" fewer sensors boost system dependability. Because of this, the system design did not allow force, temperature, and absolute position feedback sensors to be used for each actuator. So that this thesis tries to rely just on velocity and positions to control the docking system, but still does not perfectly resemble NASA logic since it seems to be exclusively on positions, even if documents recovered for this work are in contradiction on this point.

During a certain mode of operation, each linear actuator limits the load that is sent to it in a way that is right for that mode. This is called control with saturation. This last feature limits the total force put on the passive ring and the structure behind it by the soft capture ring. This makes the structure safer.

This thesis work tries to implement these guidelines on control logic by proposing a substantially Proportional-Derivative (PD) control on each actuator's displacement and velocity, independent for each actuator. When it maintains this limit and gets to the state machine's trigger for the next phase, this behavior continues up to the maximum force for that particular mode.

In particular, lunge and attenuation are here briefly presented:

- LUNGE: a predetermined pace is set as soon as contact is detected, moreover, the extension rate of each linear actuator is inversely proportional to the resistance experienced when attempting to extend. When a linear actuator meets resistance, it slows down from the "no-load" rate of extension that was told to it. The no-load lunge rate of the actuator, the maximum or "slip" force level, and the connection between the resistance encountered and the extension rate are all parameters of this mode of operation.
- ATTENUATION: after the lunge, linear actuators must maintain a position and permit a small amount of movement until a defined force limit is achieved, at which point the actuator is reversed until the applied force is reduced. After slippage has occurred, the actuator must maintain a position delta corresponding to the distance slipped.

In general, a function on an actuator's relative displacements u like the one here presented was adopted, even if this is not the implemented one, it is good to grasp the subsequent problem arising from a straightforward formulation of the NASA guidelines.

$$\begin{cases} F = k_p(u - u_{target}) + k_d(\dot{u} - \dot{u}_{target}) & \text{if } |F| < F_{max} \\ F = F_{max} & \text{if } |F| \geq F_{max} \end{cases} \tag{4.1}$$

This control logic is defined in each mode, changing each characteristic parameter, so k_p, k_d, u_{target}, $\dot{u}_{target}$ and F_{max} are state-dependent.

4.3. Smoothness Problem

The control logic stated in the previous paragraph describes a linear dependence around the $(u_{target}, \dot{u}_{target})$ line, up to the maximum admissible force, when it changes this linear behavior to a constant one, suddenly.

It is clear that a sudden change in the control logic will create some troubles in the numerical computation, first of all, because at the turning point, the derivatives are not defined, and some solutions were explored to overcome this issue.

Control laws can be written as linear functions with a limiting threshold that represents saturation in the response, but doing so means there will be some discontinuities. In order to find a solution to this problem, the following scenarios were investigated:

1. making use of some linking polynomials all the way up to a finite continuity of class n;
2. to optimize a parametric sigmoid function with the constraints of zeros and slopes, with the goal of minimizing the approximation error;
3. to locate an effective mollifier by making use of the results of Urysohn's lemma.

The first method includes at least $2N(n+1)$ parameters for each of the N discontinuity points (surfaces for higher dimensions) and each of the n continuity classes.

The second strategy's manipulation of the sigmoids did not have enough degrees of freedom to simultaneously recover the slope in the zeros locus and the "time" to reach steady conditions.

The new sigmoidal proposed by Liying Cao [10] is promising, but the fact that this function recovered their coupled parameters using constrained global optimization meta-heuristic techniques like Differential Evolution (DE) hinders their development of a potentially useful function.

Three other sigmoidal patterns covered are stated below, they both suffer from the aforementioned problems:

$$\begin{aligned} F &= k_1 \tanh(k_2 x - k_3) + k_4; \\ F &= k_1 + \frac{k_2 - k_1}{(k_3 + k_4 \mathrm{e}^{-k_5 x - k_6})^{1/k_7}}; \\ F &= k_1 \mathrm{e}^{k_2 \mathrm{e}^{k_3 (x - k_4)}} + k_5; \end{aligned} \tag{4.2}$$

It is useful to stress here the conditions and constraints that such a parametric smooth function shall accomplish:

1. At infinite its behavior shall not differ from the constant behavior of the original piecewise-linear function: $|f(\mathbf{x} \to \infty, \mathbf{k})| = F_{max}$.
2. Its value at the discontinuity point shall be tunable: $f(\mathbf{x} = \hat{\mathbf{x}}, \mathbf{k}) = \lambda F_{max}$. Otherwise, an optimality constraint shall be imposed such as minimizing the squared mismatches.
3. Its value should be the same as the value of the original piecewise-linear function in a certain part of the domain (in zero's loci in this case): $f(\mathbf{x} = \mathbf{x}_0, \mathbf{k}) = \tilde{f} = 0$.
4. In the same loci its slope shall be the same as the original piecewise-linear function: $f(\mathbf{x} = \mathbf{x}_0, \mathbf{k})_{|\mathbf{x}} = \boldsymbol{\alpha}$.
5. The cylindrical symmetry condition with respect to the zero's loci line: $f(-(\mathbf{x} - \mathbf{x}_0), \mathbf{k}) = -f((\mathbf{x} - \mathbf{x}_0), \mathbf{k})$.

Note that at least 5 parameters are required, even if some constraints can be relaxed if an optimality method like the least squares method is implemented.

The third strategy ought to be effective; however, it should make it possible to avoid direct convolution and integration in the software, and it ought to provide directly tunable flexibility.

The application of a linear description, in accordance with Victor M. Jimenez-Fernandez [11] and O. Chua's works [12–14, 21], offers an n-dimensional infinite continuity class function with a tunable error that can be managed with just one parameter more than the bare minimum set for piece-wise functions (canonical representation, which is different from the already used standard system notation).

Ochua canonical representation followed these steps to provide its compact formulation.

- Given $f = f(\mathbf{x})$ with $\mathbf{x} \in \mathbf{R}^n$.
- Defined the i-th linear partition of $\mathbf{R}^n$ such as $\boldsymbol{\alpha}_i^\top \mathbf{x} = \beta_i$.
- Given the non-degenerate partition of $\mathbf{R}^n$ in p hyperplanes.
- Defined the pseudo-unbounded, essentially-unbounded regions $\mathbf{R}_{j\infty}$ and their amount number k.
- Defined two adjacent regions associated with the i-th hyperplane where their sign-sequence vectors differ only at the i-th position as $\mathbf{R_{i+}}$ and $\mathbf{R_{i-}}$.

It is possible to establish the canonical form such as:

$$\begin{aligned}
\mathbf{b} &= \frac{1}{k}\sum_{j=1}^{k}\nabla f(\mathbf{x})\Big|_{\mathbf{R_{j\infty}}} \\
c_i &= \frac{1}{2}\frac{\boldsymbol{\alpha}_i^\top(\nabla f(\mathbf{x})|_{\mathbf{R_{i+}}} - \nabla f(\mathbf{x})|_{\mathbf{R_{i-}}})}{\boldsymbol{\alpha}^\top\boldsymbol{\alpha}} \\
a &= f(\mathbf{0}) - \sum_{i=1}^{p} c_i|\boldsymbol{\beta}_i| \\
f(\mathbf{x}) &= a + \mathbf{b}^\top\mathbf{x} + \sum_{i=1}^{p} c_i|\boldsymbol{\alpha}_i^\top\mathbf{x} - \beta_i|
\end{aligned} \tag{4.3}$$

From this notation, exploiting the work of Victor M. Jimenez-Fernandez, a smoothed representation (based on natural exponential and logarithmic functions) for the standard piecewise-linear model is presented. The result is a completely differentiable formulation with interesting properties, such as preserving the parameters of the original piecewise-linear model in such a way that they can be directly inherited to the smooth model in order to determine their parameters, the ability to control not only the smoothness grade, but also the approximation accuracy at specific break-point locations, and a low overshooting for high order derivatives.

$$\begin{aligned}
A &= a - \sum_{i=1}^{p} c_i\beta_i \\
B &= b + \sum_{i=1}^{p} c_i \\
C_i &= \frac{2c_i}{\lambda} \\
\hat{B} &= B + \sum_{i=1}^{p} c_i\boldsymbol{\alpha}_i \\
f(\mathbf{x}) &= A + \hat{B}^\top\mathbf{x} + \sum_{i=1}^{p} C_i ln\left(1 + \mathrm{e}^{\lambda(\boldsymbol{\alpha}^\top\mathbf{x}-\beta_i)}\right)
\end{aligned} \tag{4.4}$$

This notation has some overflow problems, which are solved by using a multi-objective optimization approach. This approach tries to minimize both the approximation error and the governing parameter by utilizing a weighted utopia method.

The method tries to minimize the error of the approximation while minimizing the λ parameter. Analytically it can be useful the relation between the max error e_{max} and λ,

even if a least square method comprehensive of the error distribution and along the whole domain shall be addressed.

$$e_{max_i} = \frac{2c_i ln(2)}{\lambda_i} = ln(2)C_i \tag{4.5}$$

Another way should be to avoid dealing directly with too big numbers in the exponents since quickly become NaN or inf for the machine. Moreover, even if it is a sum of addends and they are symmetric, overflow rises up just in one of the two constant thresholds, this suggests that a wise formulation can overcome these problems, in a fashion like Battin's formulation for the difference between big numbers or maybe exploiting their symmetry properties. A different approach should be to set a limiting error and in the region where it is obtained (between smooth approximation and original function) switch to the original formulation or, also, define a convergent smooth approximation to a defined locus, where to switch the formulations without errors, however in this way each parametrization requires a unique set of locii.

The resulting equations for this specific application are shown.

- Given two breaking lines so $p = 2$:

$$\begin{aligned} h_1: \quad & k_1(u - u_0) + k_2(\dot{u} - \dot{u}_0) = -F_{max}; \\ h_2: \quad & k_1(u - u_0) + k_2(\dot{u} - \dot{u}_0) = F_{max}; \\ & \boldsymbol{\alpha}_1 = [k_1, k_2]^\top; \\ & \boldsymbol{\alpha}_2 = [k_1, k_2]^\top; \\ & \beta_1 = -F_{max} + k_1 u_0 + k_2 \dot{u}_0; \\ & \beta_2 = F_{max} + k_1 u_0 + k_2 \dot{u}_0; \end{aligned} \tag{4.6}$$

- Given two essentially unbounded regions, $k = 2$
- Defining:

$$\begin{aligned} \mathbf{R}_{1\infty} &= \mathbf{R}_{1-}; \\ \mathbf{R}_{2\infty} &= \mathbf{R}_{2+}; \\ \mathbf{R}_{1+} &= \mathbf{R}_{2-}; \end{aligned} \tag{4.7}$$

- Computing:

$$\begin{aligned} f_{|\mathbf{x}}|_{\mathbf{R}_{1-}} &= \mathbf{0}; \\ f_{|\mathbf{x}}|_{\mathbf{R}_{1+}} &= f_{|\mathbf{x}}|_{\mathbf{R}_{2-}} = [k_1, k_2]^\top; \\ f_{|\mathbf{x}}|_{\mathbf{R}_{2+}} &= \mathbf{0}; \end{aligned} \tag{4.8}$$

The canonical representation, with the minimum parameter set, is defined as:

$$\begin{aligned} \mathbf{b} &= \mathbf{0}; \\ c_1 &= 1/2; \\ c_2 &= -1/2; \\ a &= f(\mathbf{0}) - \frac{1}{2}|-F_{max} + k_1 u_0 + k_2 \dot{u}_0| + \frac{1}{2}|F_{max} + k_1 u_0 + k_2 \dot{u}_0|; \end{aligned} \tag{4.9}$$

$$\begin{aligned} f(\mathbf{x}) = \Big\{ & f(\mathbf{0}) - \frac{1}{2}(|k_1 u_0 + k_2 \dot{u}_0 - F_{max}| - |k_1 u_0 + k_2 \dot{u}_0 + F_{max}| + \\ & - |k_1(u - u_0) + k_2(\dot{u} - \dot{u}_0) + F_{max}| + |k_1(u - u_0) + k_2(\dot{u} - \dot{u}_0) - F_{max}|) \Big\}; \end{aligned} \tag{4.10}$$

It is now provided the actual implemented non-linear control law:

$$\begin{aligned} A &= f(\mathbf{0}) + F_{max} - \frac{1}{2}|-F_{max} + k_1 u_0 + k_2 \dot{u}_0| + \frac{1}{2}|F_{max} + k_1 u_0 + k_2 \dot{u}_0|; \\ \hat{\mathbf{B}} &= \mathbf{0}; \\ C_1 &= 1/\lambda; \\ C_2 &= 1/\lambda; \end{aligned} \tag{4.11}$$

$$\begin{aligned} f(\mathbf{x}) = \Big\{ & f(\mathbf{0}) + F_{max} - \frac{1}{2}(|k_1 u_0 + k_2 \dot{u}_0 - F_{max}| - |k_1 u_0 + k_2 \dot{u}_0 + F_{max}| + \\ & - \frac{2}{\lambda} ln(1 + \mathrm{e}^{-\lambda(k_1(u-u_0) + k_2(\dot{u}-\dot{u}_0) + F_{max})}) + \\ & + \frac{2}{\lambda} ln(1 + \mathrm{e}^{-\lambda(k_1(u-u_0) + k_2(\dot{u}-\dot{u}_0) - F_{max})}) \Big\}; \end{aligned} \tag{4.12}$$

For a two-dimensional control law, the number of parameters of this formulation is the minimum one, just seven: $f(\mathbf{x})$, F_{max}, u_0, $\dot{u}_0$, $\lambda_1 = \lambda_2 = \lambda$, k_1 and k_2. This function is tunable and respects all the constraints stated before. Notice that just one parameter, λ, is the added parameter to enforce the infinite order smoothness, while selecting a linking polynomial, for just the continuity of the second order, shall imply ten more parameters in one dimension, with this control law tuned for each docking mode it implies 70 parameters

more than the already required, against just seven. Tuning all the parameters could quickly become quite difficult.

This result is possible for an n-linear description, if the segments of the control law were not linear the exploitation of Urysohn's lemma shall be required, roughly following these steps, defining an $h(x)$ function that smoothly joints two other functions $f_1(x)$ and $f_2(x)$ from a to b [22, 23]:

- Defining:
$$l(x) = \frac{x-a}{b-a}; \tag{4.13}$$
- Stating:
$$\begin{cases} \psi(x) = \mathrm{e}^{-1/l(x)} & if \;\; x > 0 \\ \quad = 0 & if \;\; x \leq 0 \end{cases} \tag{4.14}$$
- Computing:
$$\begin{cases} \phi(x) = 0 & if \;\; x < a \\ \quad = \dfrac{\psi(x)}{\psi(x) + \psi(1 - l(x))} & if \;\; a < x < b \\ \quad = 1 & if \;\; x > b \end{cases} \tag{4.15}$$
- The mollified function becomes:
$$h(x) = f_1(x) + \phi(x)(f_2(x) - f_1(x)); \tag{4.16}$$

This approach is not studied in this thesis work, it shall be implemented in n-dimensions and a wise choice of cutting points shall be done. Moreover, not all the functions can be mollified in this way, besides their dimensions.

Another interesting result of the canonical representation with the work of Victor M. Jimenez-Fernandez is the formulation of a new one-dimensional sigmoidal function that can overcome the issues stated for the function proposed by Liying Cao and colleagues, the tanh expression, the generalized logistic function, and the Gompertz function, supplying the smallest possible group of parameters that must be met in order to accomplish the desired level of flexibility, along with decoupled parameters that have clear definitions. The initial guess is more guessable as a result of this, and the process of optimizing the data fit is made more simple.

$$\begin{aligned} x_1 &= \frac{F_1}{m} + x_0; \\ x_2 &= \frac{F_2}{m} + x_0; \end{aligned} \tag{4.17}$$

$$\begin{aligned} f(x) = \Big\{ & F(x=0) - \frac{m}{2}(|x_1| - |x_2| + x_1 - x_2) + \\ & + \frac{m}{\alpha_1} ln(1 + \mathrm{e}^{-\alpha_1(x-x_1)}) - \frac{m}{\alpha_2} ln(1 + \mathrm{e}^{-\alpha_2(x-x_2)}) \Big\}; \end{aligned} \tag{4.18}$$

Where there are just seven parameters, $F(0)$, F_1 for the lower asymptote, F_2 for the upper asymptote, m for the slope in x_0, x_0 the zero passing point and α_1 and α_2 complying for the curvature in the slope change points. If symmetry is imposed and required just four remain, $F(0)$, F_{lim}, m, α.

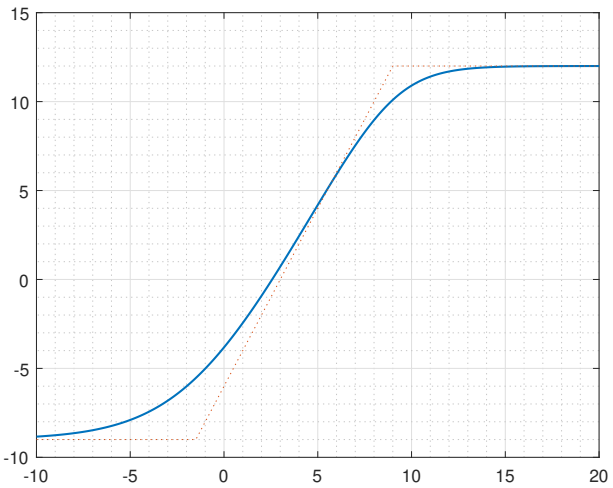

Figure 4.1: Example of a non-symmetric tunable sigmoid, computed by the presented formulation

Note that now the PD controller is no more fully actuated, since there is a saturation behavior, this implies that the controller does not follow in a straight manner the wanted conduct and the parameters characterization becomes more difficult, less predictable, and specific for the situation. To overcome these troubles it is suggested to start the modelization with a normal PD controller and then tune it with NASA guidelines. Moreover, a tuning algorithm shall be addressed in future developments.

Below are stated the control parameters required by this docking modelization.

Subsequntly, the presented graphs aim to expose and visualize the surface $f(\mathbf{x})$ that controls the actuation, before and after the smoothing process in the domain where the

variables' range can realistically be delimited. The first three figures show an exaggerated smoothing, which provides a better understanding of the process, the last instead is what shall be one of the controlling functions actually implemented.

STATE	k_1 $[N/m]$	k_2 $[Ns/m]$	λ $[-]$	F_{max} $[N]$	u_0 $[m]$	$\dot{u}_0$ $[m/s]$
EXTRACTION	2000	200	0.02	200	0.3	0
LUNGE	20	2000	0.02	67	0.4	0.1016
ATTENUATION	20000	50	0.02	356	0.05	0
ALIGNMENT	6000	5850	0.001	200	*statemachine*	0
RETRACTION	$4 \cdot 10^6$	$4.4 \cdot 10^6$	0.0001	1200	*statemachine*	0

Table 4.1: control parameters

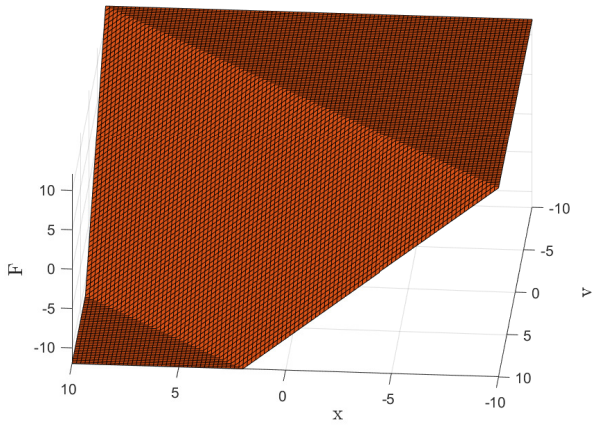

Figure 4.2: Control law directly from NASA. Dummy control laws for understanding

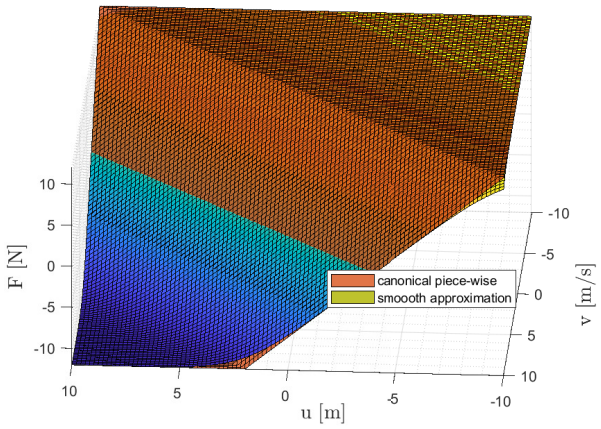

Figure 4.3: Control law after smoothing process. Dummy control laws for understanding

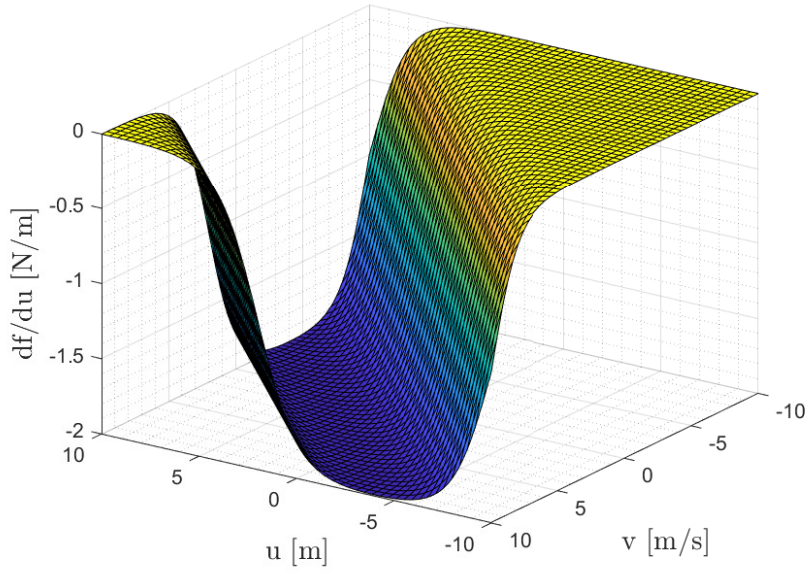

Figure 4.4: First derivatives along the position. Dummy control laws for understanding

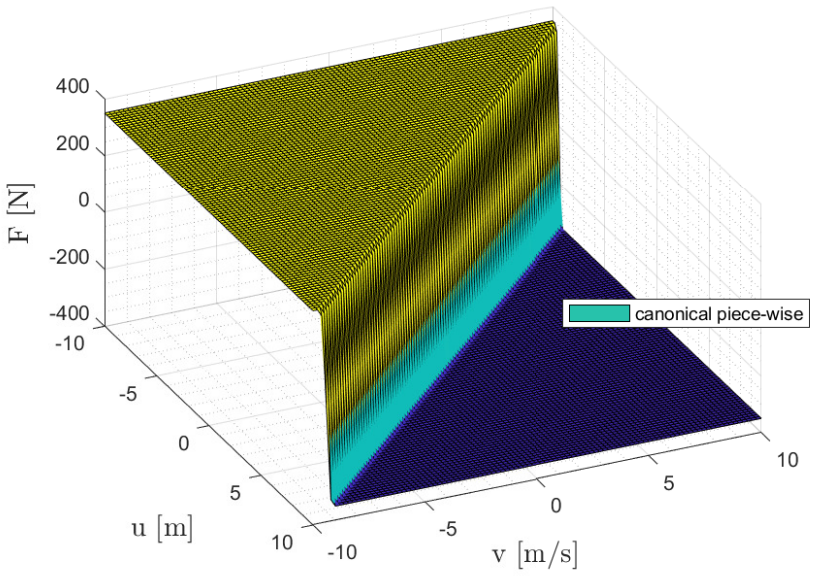

Figure 4.5: Implemented smoothed control law

5 | Simulations

5.1. Simulation's Hierarchy

The model in this thesis is built by dividing the problem into three key elements:

- Principal bodies definition and trajectories;
- Linear Actuator modelization with its control law;
- Contact interactions.

Each part is tested and simulated separately from the other parts of the system, from its simplest model to its full version. This workflow implies:

- for the principal bodies definition:
  - Bodies definition;
  - Bodies simple connection via elastic constitutive law;
  - Simple constant motion;
  - Driven motion with commanded free drift (GNC off).
- for Linear Actuator modelization with its control law:
  - A single actuator driving the system movements;
  - The Stewart platform disposition of the six actuators;
  - The simulation of the single mode of the state machine;
  - The simulation with a simple contact point, triggering the whole state machine.
- for contact interactions:
  - Single contact driving a Rod element;
  - Single contact driving a deformable displacement element, normal direction contact;

  - Finite contact area, inclined contact with respect to the normal direction;
  - Single edge contact with 30 contacts points, on the rigid bodies;
  - Full three-dimensional geometry of the contact edges attached to the mating bodies.

Verifying all the previous steps allows for proceeding with the integration of the whole system the steps are:

- to begin with the control law inclusion with the bodies, firstly with just the mating systems masses and inertia, then with the spacecraft properties;
- to include contact with the model, starting with rod-driven contacts, then with the full contact geometry.
- to simulate the whole system with all the interactions, in nominal and off-nominal situations

5.2. Results and Comments

The outcomes of this modeling are presented in this section; the incoming velocity to the target is set to be $v = 0.0368[m/s]$ in the direction of the approach. Different masses, ranging from $300kg$ to $5000kg$, and relative inertias are simulated, and a first off-nominal characterization is provided by tilting the incoming spacecraft by 2 degrees with respect to the $\hat{x}$ axis, which represents the direction from which the spacecraft is approaching. The simulations impose a total joint that forces the HCS and SCS bodies to maintain their relative alignment and direct all of the motion to the chaser vehicles. These limitations will be eliminated as a result of further development.

All of the simulations are presented with the same set of control parameters in order to place an emphasis on the performances and ranges of the model in order to move closer toward the ultimate goal of developing a generic tool. In a more detailed simulation, where the fine control will be performed, this will change. In this situation, the customizability of the module, and MBDyn in general, allows for a more precise definition of control parameters and overcome the existing limitations.

The first two plots display the approaching direction in the nominal situation, simulating the mass of the docking system by itself ($300kg$), from the perspective of the vehicle that is traveling to the space station, and from the relative displacement of the actuator. The findings illustrate a position profile that elucidates the successful completion of the full docking. Although it is possible that uncontrolled situations could arise as a result of

simulating different weights with the same control, fortunately, this has not occurred: the control is robust enough.

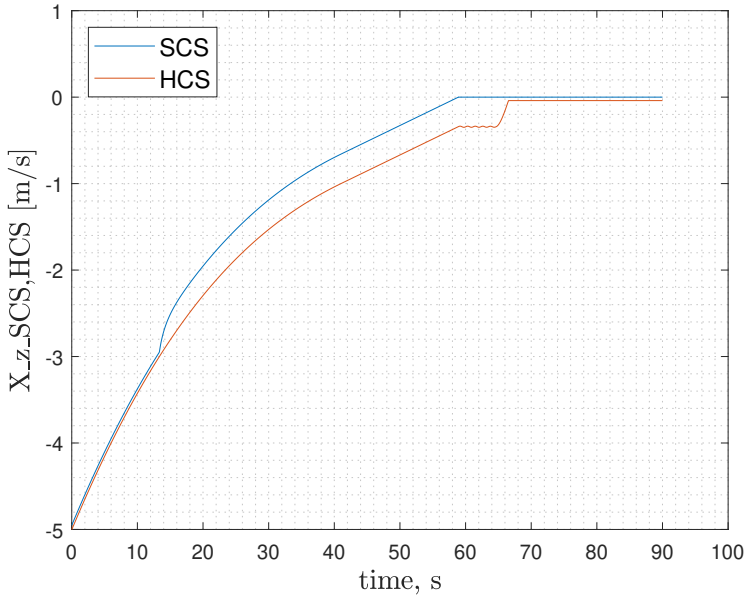

Figure 5.1: HCS and SCS pos. along incoming axis. Positions for nominal 300 kg simulation

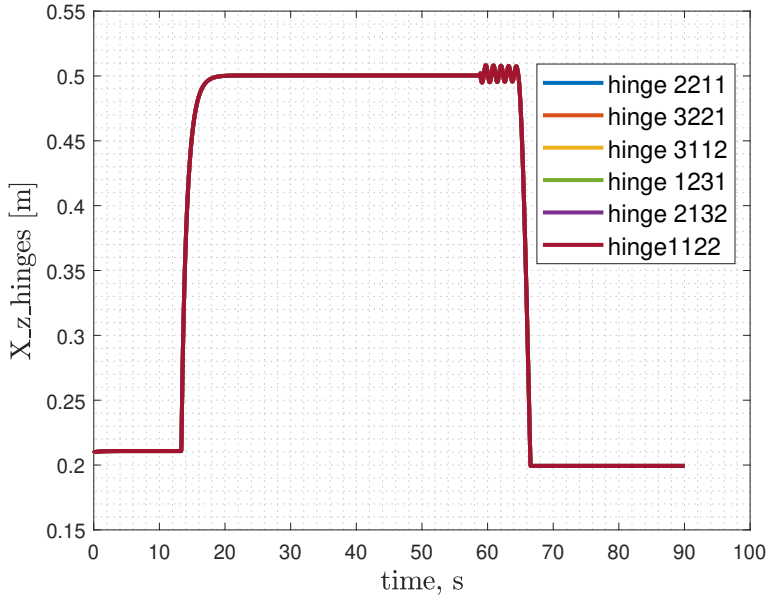

Figure 5.2: Relative motion of all actuators. Positions for nominal 300 kg simulation

The control forces and relative velocities of the actuators are displayed in the following graphs. Even if the forces are embedded with respect to the prescribed forces stated by

NASA, it must be addressed that in this light configuration, forces oscillate a lot, and this can become a challenge to overcome. The velocities are quite low all over, and while there are oscillations, they do not have a large range of movement.

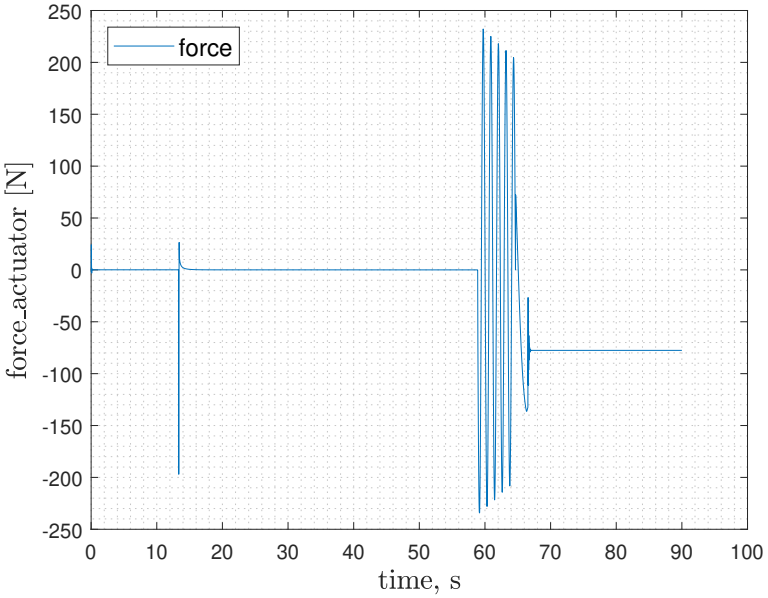

Figure 5.3: Actuator force for nominal 300 kg simulation

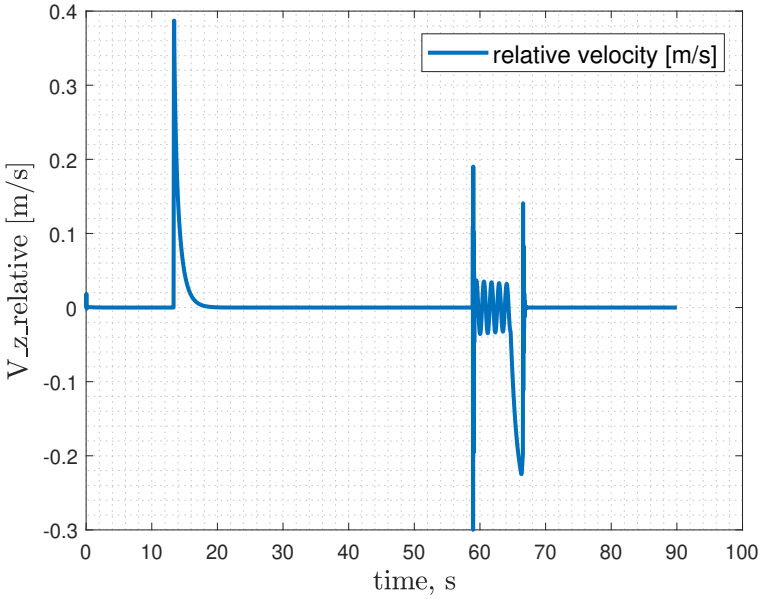

Figure 5.4: Actuator relative velocity for nominal 300 kg simulation

The off-nominal situation in general, along with the plot of the positions, demonstrates that even in this situation the simulation provides good results and the docking is achieved.

Additionally, a comparison zoom over the attenuation mode is provided, which is an important moment during which the system is highly stressed and the differences between nominal and off-nominal are more visible.

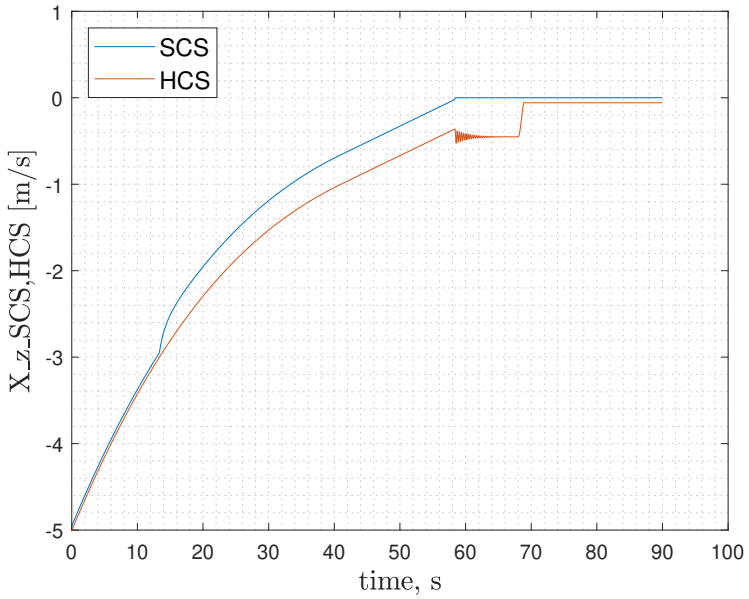

Figure 5.5: 300 kg off-nominal HCS and SCS displ. Off-nominal general behavior

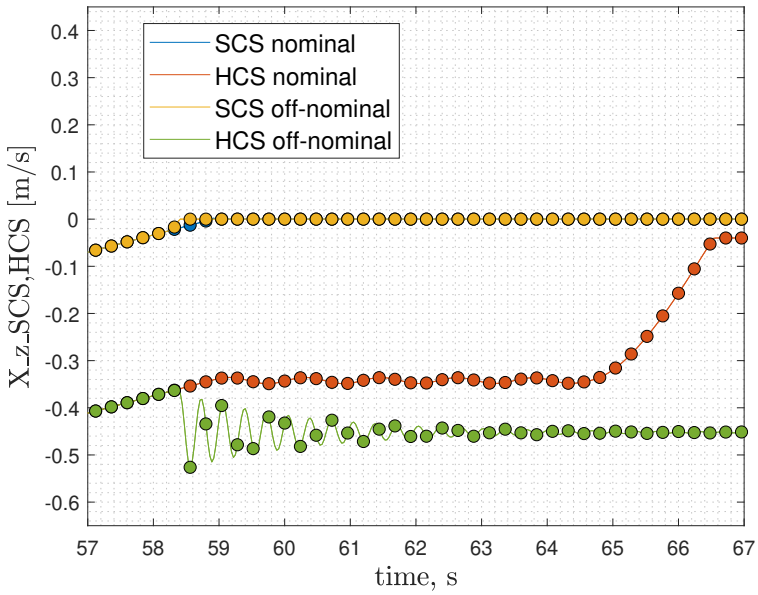

Figure 5.6: Zoom & comparison in atten. mode. Comparison with nominal simulation

Below is a presentation of the configuration with 5000 kg of mass; it is already in an off-nominal situation and does not have any constraints placed on the path of the spacecraft,

which increases its generality. The docking that was achieved can still be seen in the plots. It is presented also in the same comparison to the off-nominal value of 300 kg.

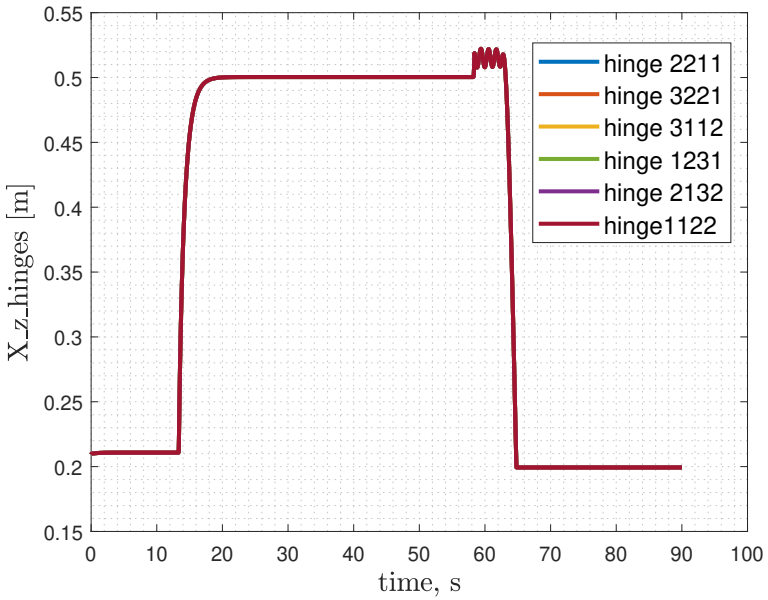

Figure 5.7: Relative actuator displacements. Off-nominal, 5000 kg simulation

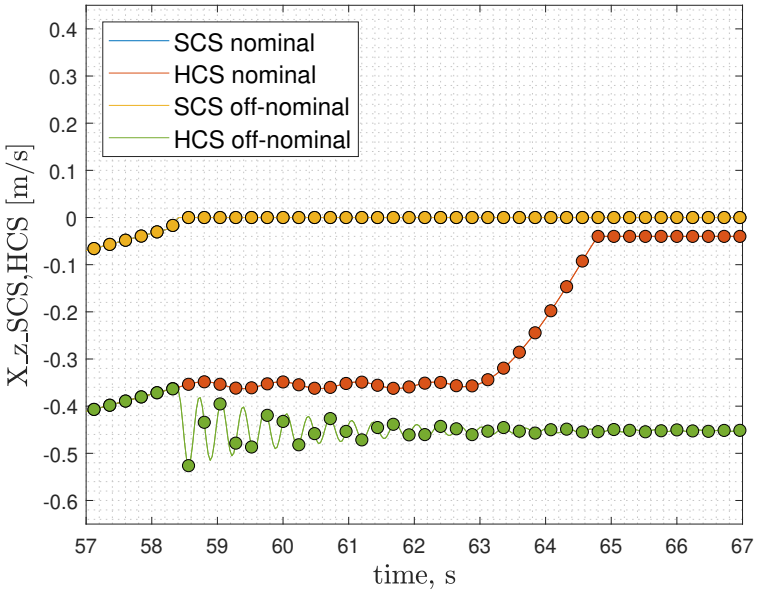

Figure 5.8: Comparison between different masses. Off-nominal, 5000 kg simulation

Some final remarks on the simulations are provided comparing the off-nominal and nominal situations for the, at this stage, most free simulations and more realistic input. The first comparison shows that in both cases the simulated situation brings to the mating of

the two spacecraft's mechanisms.

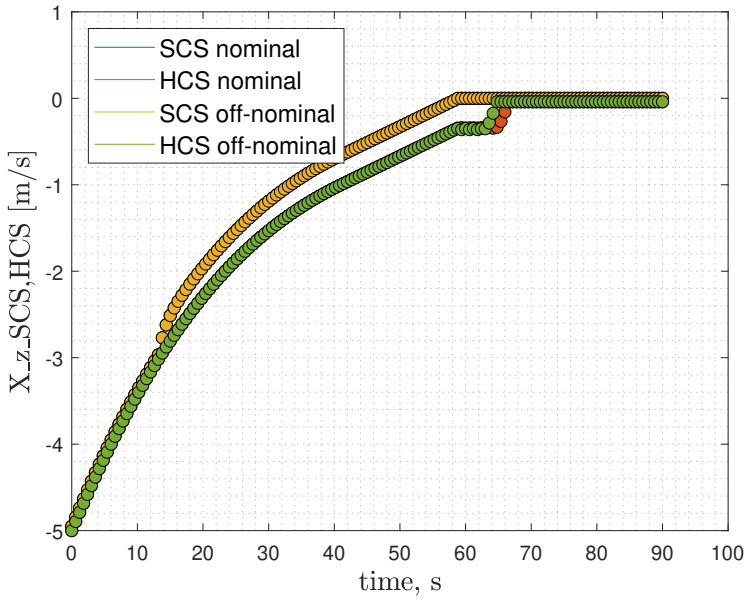

Figure 5.9: Comparison between displacements of the same mass in nominal and off-nominal, 5000 kg simulation

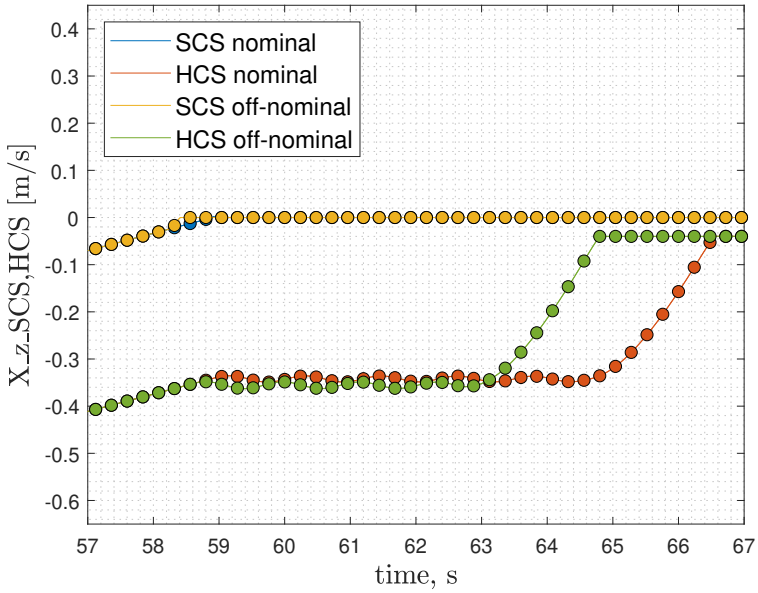

Figure 5.10: Zoom over attenuation mode between displacements of the same mass in nominal and off-nominal, 5000 kg simulation

In these two graphs displayed below it is shown the zoom in the attenuation mode. After the first contact and the relative Lunge mode actuation, the spacecraft reaches the first

soft mating, where the incoming displacement with respect to the hosting vehicle is locked by the activation of the latches and strikers system. The relative displacement in the other two directions, the pitch and yaw angles are constrained by the presence of the ring and the interaction between petals and rings. The roll angle is constrained by the interactions of the active and passive petals. At this point, a soft clamp is provided by the real system and it is simulated with the activation of a driven total joint. This activation triggers the attenuation mode and, in the velocity plot, it is evident that a non-real highly rigid dynamics arises from the clamp activation, the control damps this fictional behavior since its range is not wide and then controls the subsequent attenuation mode. A similar behavior affects structural mating, where the structural mating mode damps out these oscillations.

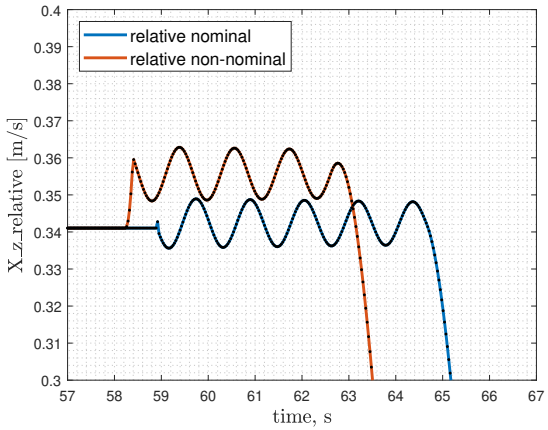

Figure 5.11: Comparison between different masses. Off-nominal, 5000 kg simulation. Zoom in attenuation mode.

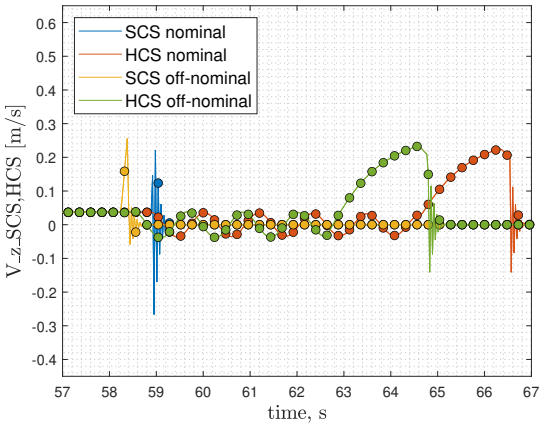

Figure 5.12: Absolute velocity comparison. Zoom over the Attenuation mode

The zoom over the velocities and over the actuation forces makes clear the state passage,

it occurs when a derivative discontinuity arises, even if the control law is totally smooth, the state machine imposes ex abrupto transitions. This is intrinsic in the definition of this state machine, a more sophisticated control and state machine shall address this problem since it can cause undesirable dynamics and it can stress the actuation bringing it to saturated behavior too early. Another aspect to stress out is the evident anticipation of the modes when in off-nominal, indeed, having an off-nominal makes the contact on the petals and not just between the latch and striker.

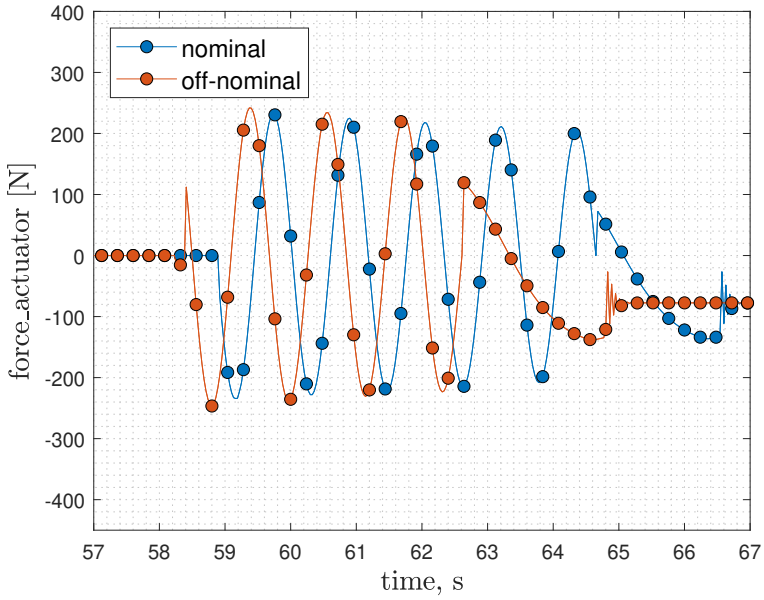

Figure 5.13: Actuator force comparison. Zoom over the Attenuation mode

About the time required for the computer, it is interesting to notice that running the two minutes long simulations on a Windows Subsystem for Linux requires roughly 20 seconds. Computer specs: processor Intel(R) Core(TM) i5-7200U CPU @ 2.50GHz, 2712 Mhz, 2 core, 4 logical processors, RAM 8.00 GB.

5.3. Improvements

The already mentioned improvements are summarized here.

From the control law point of view, it is addressed that a parameters selection method should be developed, not only, but also the control law shall overcome some issues over the overflow problem when the curvature is very high. Even the state machine shall be written imposing a smooth state transition, maybe estimating in advance the transition and linking the subsequent new control. The presented solution can be achieved via

mollifying functions, but some problems could arise as well, as the goals of each control law can tend to opposite directions, in general, an adaptive control able to change its parameters can be a solution.

The modeled system shall overcome some issues about its generality to face a wider off-nominal situation. This can be achieved by choosing a better control parametrization or reducing, as a first step, control complexity, allowing to understand if there are some criticalities in the MBDyn model or in contacts modelization.

This simulation should be placed also in algorithms for guidance or attitude control to test its performances in embedded environments and to allow a first use in integrated design.

6 | Conclusions

6.1. Line of Argument

This work provides a first tool for analysis, and with its computational velocity, the motion can be simulated in a way that is promising for embedded analysis. In fact, it already simulates some off-nominals. In their most important aspects, the NASA control laws are adhered to, although there is still room for simplifying them for preliminary research purposes.

This study is a first step in simulating a docking system using multibody dynamics with the purpose of integrating it into different space engineering fields. Following International Docking System Standards, this thesis tries to emulate docking mechanics also taking some off-nominal conditions into account. Achieving the essential balance between computational economy and accuracy in an integrated design requires exploiting MBDyn capabilities. This study tries to offer a first design instrument that incorporates docking simulation from the outset.

6.2. Future Developments

In order to make the system described here general enough to be independently implemented in a variety of algorithms, additional analysis needs to be conducted; the following problems, which will need to be solved in subsequent works, are described here.

Even though the work presented in this thesis makes the number of control parameters the fewest that it can be while still respecting NASA's guidelines for control, their number still does not allow for an easy way to select them, so a more automatic system to set them should be defined.

The model and the simulations it generates are still fairly straightforward. It does not include the complete description of the petal contact, and the motion of the spacecraft is still constrained to be nominal, with the exception of some tilting on the $\hat{x}$ axis, which constitutes a first deviation from the nominal while changing the mass is still embedded in

nominal situations. Overcoming these issues provides a more reliable tool when it comes to determining navigation trajectories or simulating control. The answers to these problems are going to have to be found in a re-characterization of the control parameters, as well as a more in-depth description of the contact. Moreover, contacts in MBDyn are not well suited, and, even if this approach works, a better formulation to reduce the number of elements required to simulate contacts shall be addressed. The implementation of line contacts or surface contacts, or the detection of them are all aspects that can improve the performance in dealing with this issue.

Another aspect to improve will be the overflow issues arising from high smoothing parameters, trying to reduce the error committed implies losing the extremities of the function, some methods to be studied are already mentioned, and here is a quick recap.

Avoid dealing directly with too big numbers, in a fashion like Battin's formulation for the difference between them. Overflow rises up just in one of the two constant thresholds, even if it is a sum of addends and they are symmetric, maybe exploiting their symmetries properties should be addressed.

Not rewriting from scratch the equation of motion of the dynamics, bu fully exploiting MBDyn with flexible elements like rods and shells could improve the embedded mechanical analysis with a first characterization of the stress flux and in this way provides the structural system with more hints to speed up a detailed analysis.

Bibliography

[1] Wigbert Fehse. *Automated Rendezvous and Docking of Spacecraft*. Cambridge University Press, Cambridge, 2003. doi:10.1017/CBO9780511543388.

[2] Sean M. Kelly and Cyran Scott P. International docking system standard (IDSS) interface definition document (IDD). Technical report, NASA, 2016.

[3] Pierangelo Masarati, Marco Morandini, and Paolo Mantegazza. An efficient formulation for general-purpose multibody/multiphysics analysis. *J. of Computational and Nonlinear Dynamics*, 9(4):041001, 2014. doi:10.1115/1.4025628.

[4] Huimin Zhang, Runsen Zhang, Andrea Zanoni, and Pierangelo Masarati. Performance of implicit A-stable time integration methods for multibody system dynamics. *MUBO*, 54(3):263–301, 2022. doi:10.1007/s11044-021-09806-9.

[5] P. Flores, M. Machado, M. T. Silva, and J. M. Martins. On the continuous contact force models for soft materials in multibody dynamics. *MUBO*, 25(3):357–375, March 2011. doi:10.1007/s11044-010-9237-4.

[6] W. J. Stronge. *Impact Mechanics*. Cambridge University Press, Cambridge, 2 edition, 2018. doi:10.1017/9781139050227.

[7] (William H. Gerstenmaier). NASA docking system (NDS) interface definitions document (IDD). Technical report, NASA, 2016.

[8] Pejmun Motaghedi and Siamak Ghofranian. Feasibility of the SIMAC for the NASA docking system. In *AIAA Space and Astronautics Forum and Exposition (SPACE 2014)*, San Diego, CA, USA, 2014.

[9] Brandon N. Dick, Christopher Oesch, and Timothy Rupp. Linear actuator system for the nasa docking system. In *European Space Mechanisms and Tribology Symposium*, Hatfield, Hertfordshire, UK, 2017.

[10] Liying Cao, Pei-Jian Shi, Lin Li, and Guifen Chen. A new flexible sigmoidal growth model. *Symmetry*, 11(2), 2019. doi:10.3390/sym11020204.

[11] Victor M. Jimenez-Fernandez, Maribel Jimenez-Fernandez, Hector Vazquez-Leal, and Evodio Muñoz-Aguirre. Transforming the canonical piecewise-linear model into a smooth-piecewise representation. *SpringerPlus*, 5(1), 2016. doi:10.1186/s40064-016-3278-y.

[12] C. Kahlert and Leon O. Chua. The complete canonical piecewise-linear representation. Technical Report UCB/ERL M89/32, EECS Department, University of California, Berkeley, Mar 1989.

[13] Leon Ong Chua and Robin L. P. Ying. Canonical piecewise-linear analysis. *IEEE Transactions on Circuits and Systems*, 30(3):125–140, 1983. doi:10.1109/TCS.1983.1085342.

[14] Leon O. Chua and An-Chang Deng. Canonical piecewise-linear representation. *IEEE Transactions on Circuits and Systems*, 35(1), Jan 1988.

[15] Finn Ankersen. *Guidance, Navigation, Control and Relative Dynamics for Spacecraft Proximity Maneuvers.* PhD thesis, Aalborg University, December 2010.

[16] O. A. Bauchau. *Flexible multibody systems: preliminaries*, pages 569–599. Springer Netherlands, Dordrecht, 2011.

[17] Werner Schiehlen. Multibody system dynamics: Roots and perspectives. *Multibody System Dynamics*, 1:149–188, 1997.

[18] P. Masarati. Multibody system dynamics. Course notes, 2022.

[19] Matteo Fancello. A co-simulation approach for mixed smooth and nonsmooth dynamics in multibody problems. Master's thesis, Politecnico di Milano, December 2012.

[20] Timothy Rupp Christopher Oesch, Brandon Dick. Multi-axis independent electromechanical load control for docking system actuation development and verification using dspace. Technical report, Moog, 2015.

[21] Leon Ong Chua and Sung Mo Kang. Section-wise piecewise-linear functions: Canonical representation, properties, and applications. *Proceedings of the IEEE*, 65:915–929, 1977.

[22] Walter Rudin. *Real and Complex Analysis, 3rd Ed.* McGraw-Hill, Inc., USA, 1987.

[23] H. Amann, G. Brookfield, and J. Escher. *Analysis I.* Birkhäuser Basel, 2009.

List of Figures

List of Tables